

UTTAC-79, 2010

UTTAC

ANNUAL REPORT 2009

TANDEM ACCELERATOR COMPLEX
Research Facility Center for Science and Technology
University of Tsukuba

<http://www.tac.tsukuba.ac.jp/>

UTTAC

ANNUAL REPORT 2009

April 1, 2009 – March 31, 2010

UTTAC-79 2010

Executive Editor: Hiroshi Kudo

Editors: Yoshihiro Yamato, Daiichiro Sekiba, Kimikazu Sasa, Tetsuro Komatsubara

UTTAC is a series of issues, which include annual reports of Tandem Accelerator Complex, Research Facility Center for Science and Technology, University of Tsukuba.

The issues may also include irregular reports written by English.

Copyright © 2010 by Tandem Accelerator Complex, Research Facility Center for Science and Technology, University of Tsukuba and individual contributors.

All reports are written on authors' responsibility and thus the editors are not liable for the contents of the report.

Tandem Accelerator Complex, Research Facility Center for Science and Technology,
University of Tsukuba

Tennodai 1-1-1, Tsukuba, Ibaraki 305-8577, Japan

<http://www.tac.tsukuba.ac.jp/>
annual@tac.tsukuba.ac.jp

PREFACE

This annual report covers researches carried out at University of Tsukuba Tandem Accelerator Complex (UTTAC) during the fiscal year 2009 (1 April 2009 ~ 31 March 2010). The topics include not only accelerator-based researches using the 12UD Pelletron and 1 MV Tandatron accelerators, but also closely related researches to UTTAC.

October 1, 2010

Editors

CONTENTS

1. ACCELERATOR AND EXPERIMENTAL FACILITIES	
1.1 Accelerator operation (2009)	1
1.2 Status of the Tsukuba AMS system (2009)	4
1.3 The developments of detectors of the particle identification for RI beam experiment	5
1.4 Development of active target with gas electron multiplier	7
2. NUCLEAR PHYSICS	
2.1 Study of the structure of ^{30}S by in-beam gamma ray spectroscopy and the $^{29}\text{P}(p,\gamma)^{30}\text{S}$ reaction rate in classical novae	9
2.2 Measurement of nuclear magnetic moment of unstable nucleus ^{40}Sc . II	11
2.3 Measurement of nuclear magnetic moment of unstable nucleus ^{30}P	13
2.4 Study of nuclear synthesis of ^{26}Al by gamma ray spectroscopy III	15
3. MATERIALS AND CLUSTER SCIENCE	
3.1 Electron emission from surfaces bombarded by MeV atom clusters	17
3.2 X-ray absorption spectroscopy of Mg-Ni and Mg-Ti hydride	19
3.3 The vicinage effect on energy loss of C_2^+ in a thin carbon foil	21
3.4 Study on nitrogen diffusion in $\epsilon\text{-Fe}_{2-3}\text{N}$ submicron particles	23
4. ACCELERATOR MASS SPECTROMETRY	
4.1 Fluctuations in cosmic ray flux around 11 kyr BP based on cosmogenic ^{36}Cl from the Dome Fuji ice core	27
4.2 Distribution of ^{36}Cl in the Yoro River basin and its relation to regional groundwater flow system	28
4.3 Measurement of ^{36}Cl in soil : Study of extraction methods according to reservoirs	30
4.4 Chlorine-36 produced in muon irradiation	32
4.5 Production rates of ^{36}Cl for target elements in chondritic meteorites (II)	34
5. INTERDISCIPLINARY RESEARCH	
5.1 Trace-element analysis of fluid inclusions in the Tsushima granite, Japan	37
5.2 Nanopore fabrication by irradiating accelerated ions for high-sensitivity waveguide-mode sensors	39
6. LIST OF PUBLICATIONS	
6.1 Journals	41
6.2 International conferences	45

7. THESES	48
8. SEMINARS	49
9. SYMPOSIA	51
10. LIST OF PERSONEL	58

1.

ACCELERATOR AND EXPERIMENTAL FACILITIES

1.1 Accelerator operation (2009)

K. Sasa, S. Ishii, H. Kimura, H. Oshima, Y. Tajima, T. Takahashi, Y. Yamato,
T. Komatsubara, D. Sekiba and H. Kudo.

The total service time of the UTTAC multi-tandem accelerator facilities was 146 days (3,504 hours) in the fiscal year 2009. 15.8 % (552 hours) of the total service time was used for industrial users, under the project "Open Advanced Facilities Initiative for Innovation (strategic use by industry)", which was supported financially by the Ministry of Education, Culture, Sports, Science and Technology.

The 12UD Pelletron tandem accelerator

The operating time and the experimental beam time of the 12UD Pelletron tandem accelerator were 1705 and 1226.4 hours, respectively, during the fiscal year 2009. Fig.1 shows the accelerator operation hours per month. Fig.2 shows the beam time histogram with respect to the terminal voltage. Fig.3 represents the percentage of the operation hours for the three ion sources and ion species.

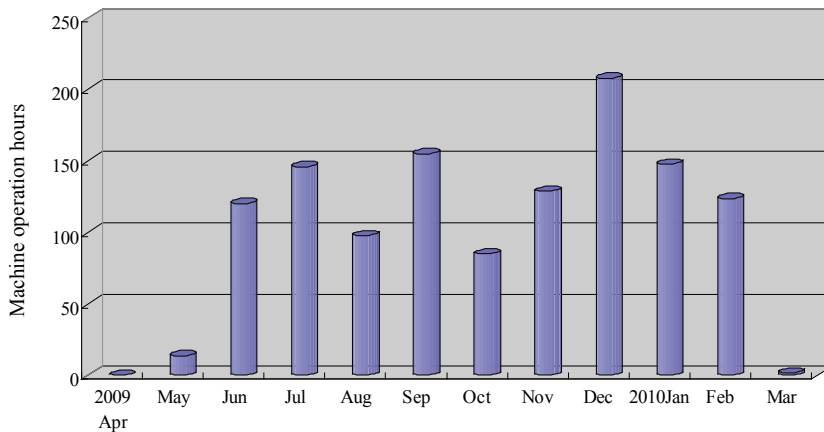


Fig.1. Accelerator operation hours per month for the 12UD Pelletron tandem accelerator in 2009.

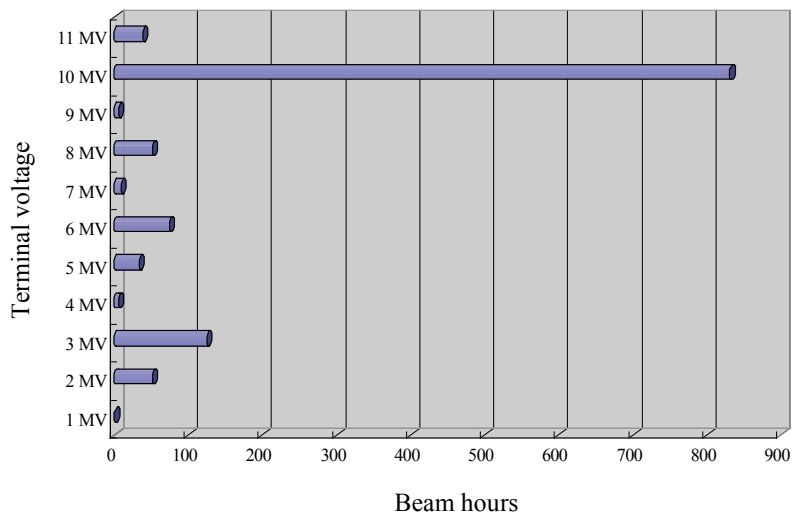


Fig.2. Beam time histogram as a function of the terminal voltage for the 12UD Pelletron tandem accelerator in 2009.

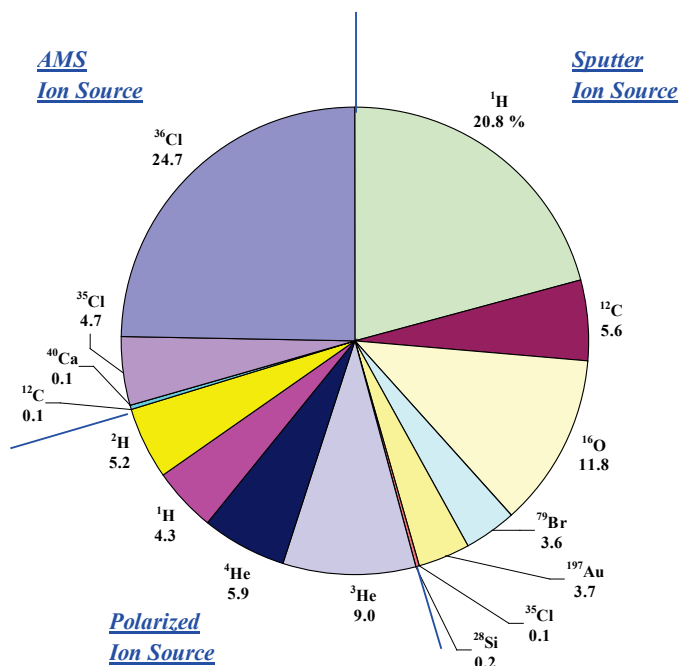


Fig.3. Percentage of the operation hours for the three ion sources and ion species in 2009.

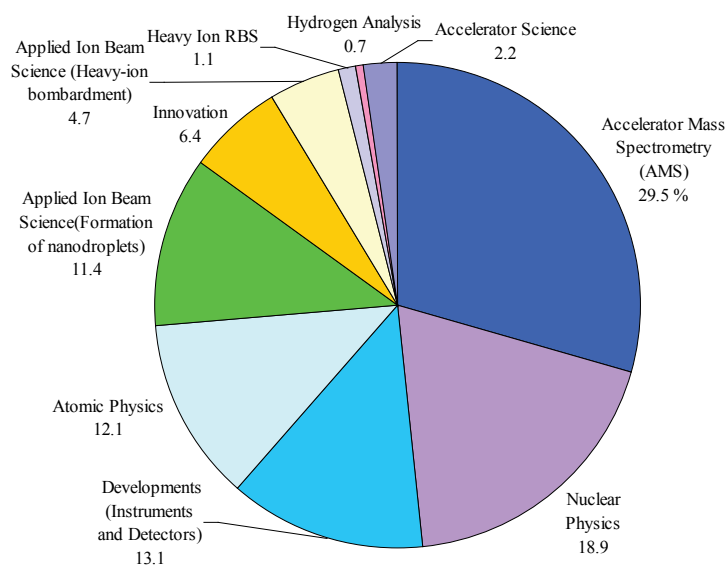


Fig.4. Percentage of the experimental beam time for the running research fields in 2009.

In 2009, 62 research programs were carried out using the 12UD Pelletron tandem accelerator. Totally, 668 researchers used the 12UD Pelletron tandem accelerator. Fig.4 shows the percentage of the experimental beam time for the running research fields with the 12UD Pelletron tandem accelerator. The periodic maintenance of the 12UD Pelletron tandem accelerator was scheduled for the spring of 2010, but was postponed on July due to the breakdown of the SF₆ gas-recovery unit.

The 1 MV Tandetron accelerator

The operating time and the experimental beam time of the 1MV Tandetron accelerator were 375.4 and 161.5 hours, respectively, during the total service time. In 2009, 40 research programs were carried out using the 1 MV Tandetron accelerator. Totally, 251 researchers used the 1 MV Tandetron accelerator. Fig. 5 shows the percentage of accelerated ions for the 1 MV Tandetron accelerator. Fig. 6 shows the percentage of the experimental beam time for the running research fields.

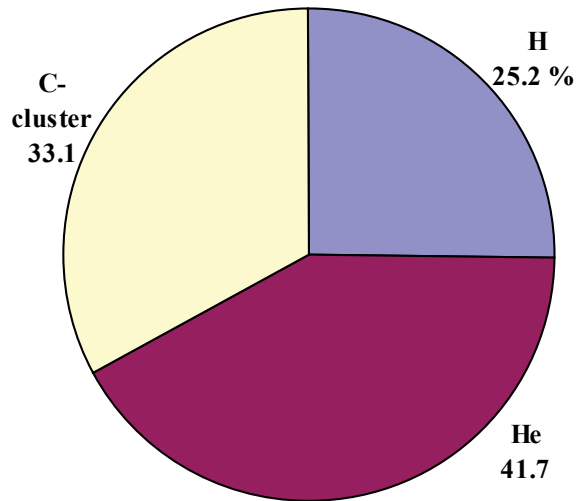


Fig.5. Percentage of accelerated ions for the 1 MV Tandetron accelerator in 2009.

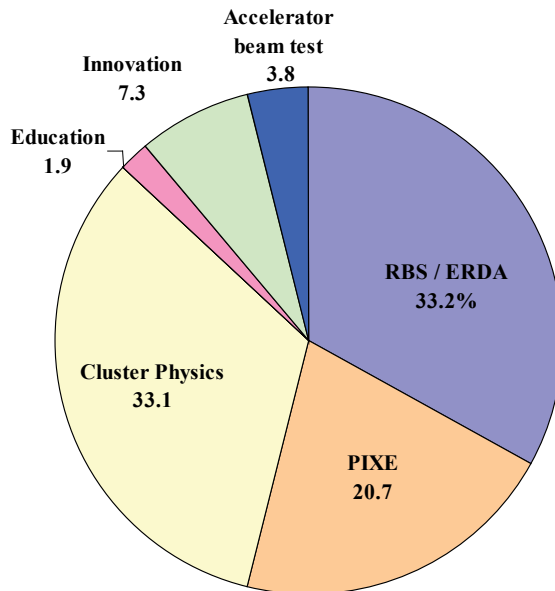


Fig.6. Percentage of the experimental beam time for the running research fields with the 1 MV Tandetron accelerator in 2009.

1.2 Status of the Tsukuba AMS system (2009)

K. Sasa, T. Takahashi, Y. Tosaki, K. Sueki, N. Kinoshita, T. Amano, J. Kitagawa, K. Kurosumi, M. Matsumura, S. Abe, Y. Nagashima, K. Bessho¹, H. Matsumura¹ and Y. Matsushi²

The Tsukuba AMS system is able to measure environmental levels of long-lived radioisotopes of ¹⁴C, ²⁶Al, ³⁶Cl and ¹²⁹I by employing a molecular pilot beam. We have focused our activities on ³⁶Cl measurements. In 2009, 309 samples for ³⁶Cl were measured by the Tsukuba AMS system. Total operation of the Tsukuba AMS system was 54 days in 2009. Table 1 shows current research programs and the number of samples in 2009.

We have measured cosmogenic ³⁶Cl in the Dome Fuji ice core, Antarctica. The apparent ³⁶Cl flux at the Dome Fuji Station was estimated approximately to be $2.5\text{--}3.5 \times 10^4$ atoms cm⁻² yr⁻¹ [1]. We have started a new project for ³⁶Cl measurements in the Greenland NEEM ice core. It is expected to discover innovative bipolar information for the paleo-environmental reconstruction. We have carried out a joint research project for ³⁶Cl exposure dating of Tiankeng in China with the China Institute of Atomic Energy. We have been developing a ⁴¹Ca AMS for future research programs. ⁴¹Ca is a cosmogenic nuclide of interest for studying the irradiation history of extraterrestrial material.

Table 1 Research programs and the number of samples by the Tsukuba AMS system in 2009.

AMS research programs	Target material	Organization	Number
³⁶ Cl-AMS ³⁶ Cl in the Dome Fuji ice core, Antarctica.	Antarctic ice core	Univ. of Tsukuba	121
Measurement of ³⁶ Cl in soil. Environmental monitoring for nuclear facilities by AMS.	Soil	Univ. of Tsukuba	48
Bomb-produced ³⁶ Cl as a tracer in groundwater.	Hydrological samples (ground water, rain water)	Univ. of Tsukuba	75
In-situ ³⁶ Cl for denudation rates of karst landform. ³⁶ Cl exposure dating for Tiankeng.	Limestone	The Univ. of Tokyo Univ. of Tsukuba CIAE	24
Production rates of Cl-36 for target elements in chondritic meteorites.	Meteorite	Tokyo Metro. Univ.	31
Chlorine-36 produced in muon irradiation.	NaCl, CaCO ₃	Univ. of Tsukuba	10
⁴¹ Ca-AMS ⁴¹ Ca-AMS development.	CaF ₂	Univ. of Tsukuba	23

References

[1] K. Sasa et al., *Nucl. Instr. and Meth. B* 268 (2010) 1193-1196.

¹ Radiation Science Center, High Energy Accelerator Research Organization

² Disaster Prevention Research Institute, Kyoto University

1.3 The developments of detectors of the particle identification for RI beam experiment

T.Moriguchi, A.Ozawa, H.Suzuki, D.Nagae, Y. Ito, H.Ooishi, Y. Ishibashi, K.Yokoyama, N.Kamiguchi, and Y.Abe

We have developed a solid-neon detector for measuring the total energy of particles in the RI beam experiments. The value of total energy of each particle is needed for particle identification of the RI beam. An NaI(Tl) detector is usually used as the total-energy detector. This detector is unsuitable for high-rate beam because of the scintillation light quenching. It is important to develop a new total-energy detector which replace the NaI(Tl) detector.

Through the interaction of radiations with noble gasses, scintillation is emitted and electron–hole pairs are produced. From these features, the noble gasses can be used as the scintillation counter and the ionization chamber. While the liquid/solid xenon/argon detectors have been studied [1], there are few studies of the liquid or solid neon detectors. One of the reasons is that it is difficult to make a liquid/solid neon because the melting point of the neon is lower than that of the xenon/argon. To solidify the neon gas, we used a cryogenic system which have been already used for developing a solid hydrogen target [2]. The purpose of this study is to investigate the properties of a neon as a scintillation and a proportional counter and to develop this detector system.

The experiment have been performed at the F-course beam line in UTTAC. Figure 1 shows a schematic view of an experimental setup and a picture of the solid neon cell. A proton beam with 21 MeV was transported to the neon detector located downstream of the Q-D-Q magnets. The beam intensity was adjusted about 1000 counts per second by scattering with a gold foil at the scattering chamber. The size of the solid neon was $\phi 50 \text{ mm} \times 30 \text{ mm}^{\dagger}$. For using as a scintillation counter, a photo multiplier tube (PMT) was equipped for detecting the scintillation. The wave length of the scintillation from the solid neon was shifted by using a tetraphenyl butadiene (TPB) for being detected by PMT. For using as a proportional counter, the copper wire which was applied a high voltage was put in the solid neon for obtaining the signals.

In this experiment, no signal from the solid neon was observed by using both counters. We are finding out the reason about the present result.

References

- [1] Glenn F. Knoll, Radiation Detection and Measurement (3rd), John Wiley & Sons, Inc.
- [2] T. Moriguchi et al., RIKEN Accel. Prog. Rep. **42** (2008) 185.
- [3] R.A. Michniak et al., Nucl. Instr. and Meth. A **482** (2002) 387.
- [4] D.N. McKinsey et al., Nucl. Instr. and Meth. B **132** (1997) 351.

@ F-course

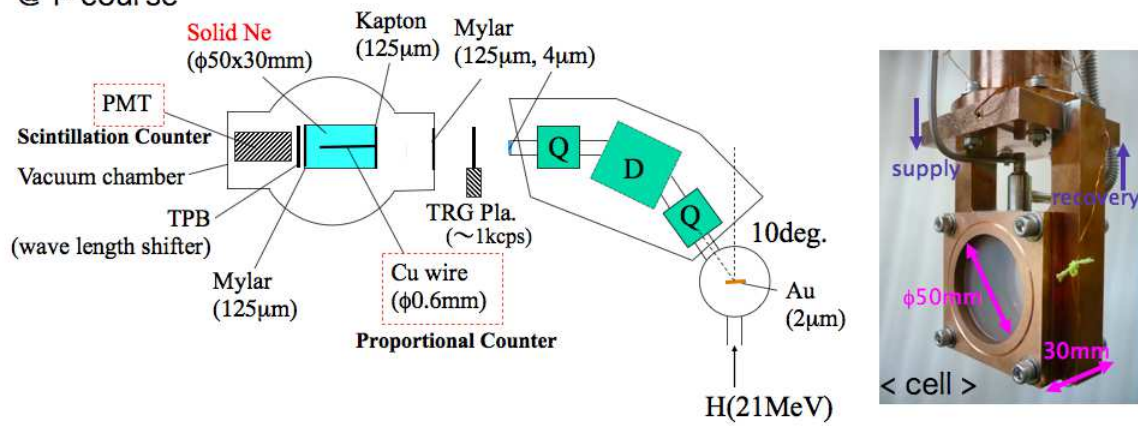


Fig. 1. The schematic experimental setup and the picture of the solid neon cell.

1.4 Development of active target with gas electron multiplier

S. Ota¹, R. Akimoto¹, T. Hashimoto¹, T. Gunji¹, S. Michimasa¹, H. Yamaguchi¹, H. Tokieda¹, T. Tsuji¹, S. Kawase¹, H. Hamagaki¹, T. Uesaka¹, S. Kubono¹, T. Isobe², T. Kawabata³, A. Ozawa, H. Suzuki, D. Nagaie, T. Moriguchi, Y. Itoh, Y. Ishibashi, H. Ooichi, and Y. Abe

We are developing two types of active targets using Gas Electron Multiplier (GEM) [1] for the experimental study with intense (10^{6-7} Hz) radioisotope beams in inverse kinematics. The active target has two functions of target and detector at the same time and enables us to measure the recoiled particle with low energy.

One type being developed is “beam transparent type” for the study of nuclear structure and property of nuclear matter by measuring the giant resonances such as monopole, dipole, and Gamow-Teller excitation via (α, α') , (d, d') or $(d, ^2\text{He})$ reactions. Missing mass spectroscopy is a powerful tool for these measurements, since such resonances are populated with high excitation and then the excited nuclei decay immediately by particle emission. Hence we need to measure the recoiled particles such as α , d and protons with low kinetic energy in the forward angle scattering, which is essential to identify the transfer momentum in the reaction. The structure of this active target is optimised as not to measure the beam particles for the high-rate beam up to 10^7 Hz with the high incident energy of 100–200 MeV/u. The detail of the structure is described later.

The other type is “beam measurement type” for the study of nuclear astrophysics, especially rp -process in nucleosynthesis. So far, the (α, p) reaction has been measured by using thick-target method in CRIB facility in RIKEN. Although the large window of excitation energy is studied at the same time by this method, there still remain some uncertainties in identification of reaction process, beam energy, and position of beam and recoiled particles. To reduce these uncertainties, we need to measure the reaction point.

We performed two experiments to evaluate the energy and position resolutions of active targets and their position dependencies for “beam transparent type” in December, 2009 and for “beam measurement type” February, 2010. In this report, the details of “beam transparent type” active target, the experimental setup and result are described.

The schematic view of the “beam transparent type” active target is shown in Fig. 1. In this figure, the typical case of physics experiment is shown, which is not the same as the setup in this experiment. The beam particles go through between two field cages to measure recoiled particles. The electrons created by the recoiled particles in the cage drift along the electric field formed by doubly layered field wires. The electrons reach at the GEM of 100 μm thickness and amplified by typically 10^3 . The charge is collected by a readout pad patterned with $16.45 \times 16.45 \text{ mm}^2$ rectangular triangle. Since there is no field along the beam path and the centroid of cross section of beam is away from field cage, the electric field in the cage is not affected by the space charge of the residual ions. Three dimensional position is deduced from the drift time and the charge division in two adjacent pads.

¹Center for Nuclear Study, University of Tokyo

²Nishina Center for Accelerator-Based Science, RIKEN

³Department of Physics, Kyoto University

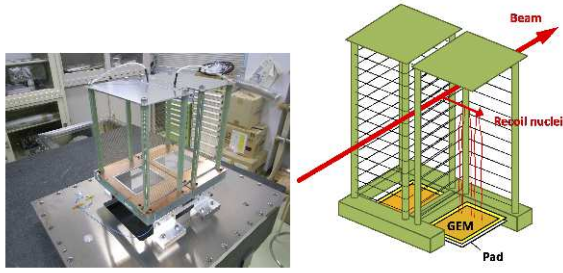


Fig. 1. Picture (left panel) and schematic view (right panel) of “beam transparent type” active target. The recoiled particles are detected in two field cages. In this experiment, the ^4He beam particles are irradiated along the direction of recoiled particles indicated in the figure.

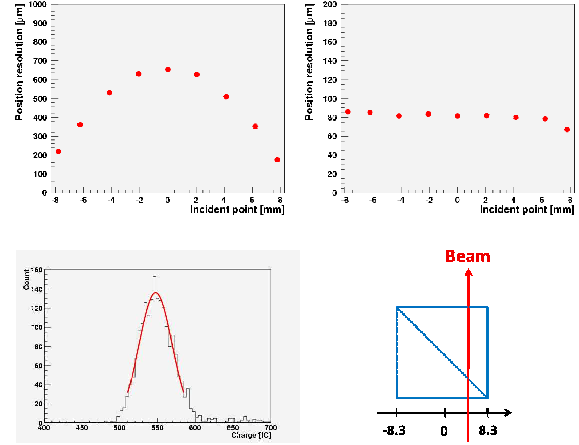


Fig. 2. Resolutions from the charge division (top left) and the drift time (top right) and their position dependencies; Energy resolution (bottom left); and definition of incident position.

The experiment was performed at the 12UD Pelletron tandem accelerator. Ion beam of ^4He was accelerated up to 30 MeV. The beam rate was adjusted to be typically 10^3 Hz by using gold-foil scatterer. The beam was irradiated from the side of the field cage, *i.e.*, the detection area was bombarded directly by the beam particle. The active target was filled with an admixture gas of He (95%) and CO_2 (5%) of atmospheric pressure and operated with 700-V/cm electric field where drift velocity of electron was about 2 cm/ μm . A voltage supplied to the GEM was adjusted so that gas gain was about 10^3 . The signal from the active target was amplified using RPA-211 (REPIC) and digitized by 100-MHz sampling flash ADC, SIS3301, (SIS). Trigger of the digitization was made by the logical OR of first 4 pads along the beam path.

Time and charge information are deduced by the pulse shape analysis of the sampled signal. First analysis has been done with simple way: the timing information is deduced from the extrapolation of rising edge and the charge information is deduced from the maximum charge assuming rise and fall time of each pulse are similar. Their position dependence are shown in Fig. 2. The ordinate and abscissa axes show the resolution and incident position with the origin at the center of the pad, respectively. The resolution from the charge division strongly depends on the incident position, however, its dependency is explained by propagation of errors of the energy deposition in two pads. On the other hand, the resolution from the drift time is independent from the incident position. The measured position resolutions are typically less than 700 μm and 80 μm from the charge division and the drift time, respectively. The calculated angular resolution is about 8 mrad.

As outlook, we plan to measure the effect of δ rays with high-energy (~ 200 MeV/u) beam and the distortion of electric field by the space charge with high-rate ($\sim 10^6$ Hz) beam.

References

- [1] M. Inuzuka et al., Nucl. Instrum. and Method A **525**, 529(2004).

2.

NUCLEAR PHYSICS

2.1 Study of the structure of ^{30}S by in-beam gamma ray spectroscopy and the $^{29}\text{P}(p,\gamma)^{30}\text{S}$ reaction rate in classical novae

K. Setoodehnia*, A. A. Chen*, T. Komatsubara[‡], Y. Sugiyama[‡], A. Ozawa[‡], T. Moriguchi[‡], Y. Ito[‡], H. Ooishi[‡], Y. Ishibashi[‡], T. Hayakawa[#], T. Shizuma[#], S. Kubono[%], H. Yamaguchi[%], T. Hashimoto[%], D. Kahl[%], D. N. Binh[%]

* Department of Physics & Astronomy, McMaster University, Hamilton, ON L8S 4M1, Canada

[‡] Institute of Physics, University of Tsukuba, Tennodai 1-1-1, Tsukuba, Ibaraki 305-8577, Japan

[#] Japan Atomic Energy Agency (JAEA), Tokai, Ibaraki 319-1195, Japan

[%] Center for Nuclear Study (CNS), University of Tokyo, Wako Branch at RIKEN, 2-1 Hirosawa, Wako, Saitama, 351-0198, Japan

Classical novae are stellar explosions resulting from a thermonuclear runaway, which occur in close binary systems consisting of a compact white dwarf and a low-mass Main Sequence companion. The dominant nova nucleosynthetic path followed by the thermonuclear runaway can be understood by analyzing the Si isotopic abundance ratios ($^{29}\text{Si}/^{28}\text{Si}$ and $^{30}\text{Si}/^{28}\text{Si}$) in presolar grains of nova origin, which are dust grains formed in the ejecta of classical novae [1]. This in turn can help to elucidate the chemical composition of the white dwarf and the thermal history of the white dwarf's convective envelope.

To calculate the Si isotopic abundances in such presolar grains, one needs to know the rates of the reactions which affect the $^{29,30}\text{Si}$ production and destruction in novae. One such reaction is the $^{29}\text{P}(p,\gamma)^{30}\text{S}$ reaction [2], whose rate depends significantly on the properties of ^{30}S resonances above the proton threshold of ^{30}S at $S_p = 4399 \pm 3$ keV [3]. However, the properties of these resonances are yet not well understood.

At the temperatures characteristic of explosive hydrogen burning in novae (0.1 – 0.4 GK) the $^{29}\text{P}(p,\gamma)^{30}\text{S}$ reaction rate is dominated by two low energy 3^+ and 2^+ resonances, whose energies were predicted to be 4733 ± 40 keV and 4888 ± 40 keV, respectively [2]. Despite several experimental studies on the structure of ^{30}S [4, 5, 6, 7, 8, 9, 10], the 2^+ level remains unobserved and the 3^+ level has only been tentatively observed to be at 4704 ± 5 keV recently [9]. Thus, the $^{29}\text{P}(p,\gamma)^{30}\text{S}$ reaction rate, which depends exponentially on the resonance energies, remains uncertain by orders of magnitude.

In order to address the remaining large uncertainty in the $^{29}\text{P}(p,\gamma)^{30}\text{S}$ reaction rate, we decided to further investigate the level structure of ^{30}S using the $^{28}\text{Si}(^3\text{He},n\gamma)^{30}\text{S}$ reaction. The first phase of this in-beam gamma-ray spectroscopy measurement was performed at UTTAC. A natural Si target of 25 μm thickness was irradiated by a 10 MeV ^3He beam. Gamma-gamma coincidence measurements were performed with two Ge-detectors with relative efficiencies of 140% and 70%. A NE-213 liquid scintillator was also employed to detect neutrons for a measurement of neutron-gamma coincidences.

Due to low neutron statistics in this first run, we could not learn much from the neutron-gamma coincidence measurement. However, as a result of the preliminary analysis of gamma-gamma coincidence measurement, we were able to observe eight levels in ^{30}S , three of which are above the proton threshold including the two levels at 4687.9 ± 0.2 keV and 4810.4 ± 0.5 keV, which likely correspond to the two

astrophysically important states predicted by Iliadis *et al.* [2]. Moreover, a state was observed at 4250.1 ± 1.4 keV which is below the proton threshold and might be a new state in ^{30}S . The origin of the newly found level is still under investigation but it decays to the second excited state of ^{30}S by emitting a 845.4 keV γ -ray (see Fig. 1). If one compares the γ -decay scheme of ^{30}S with that of its mirror nucleus ^{30}Si , one can tentatively estimate the spin assignments of the levels in ^{30}S from the relative intensities of the γ -rays. This analysis is still in progress. In order to pin down the spin/parity assignments, the next phase of the experiment will measure the Directional Correlation of Oriented (DCO) nuclei ratios of the relevant transitions.

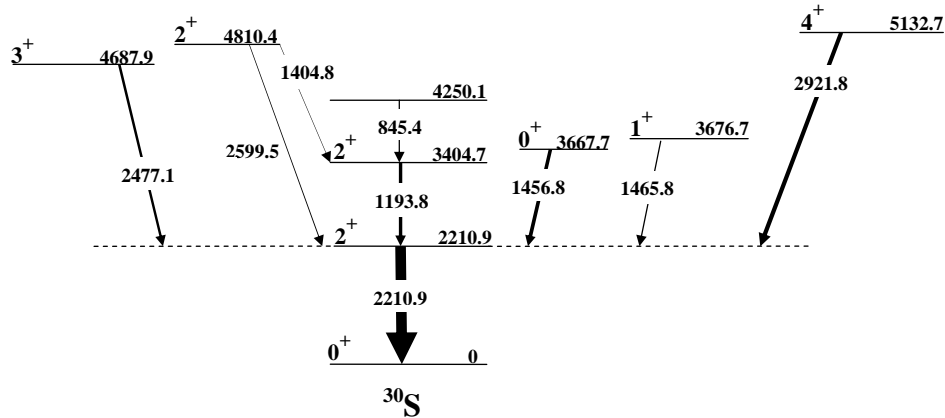


Fig. 1. The level structure of ^{30}S determined thus far in this project. The spins and parities are tentatively assigned based on comparison with the mirror levels in ^{30}Si .

References

- [1] J. José, M. Hernanz, S. Amari, and E. Zinner, *Astrophys. J.* 612 414 (2004).
- [2] C. Iliadis, J. M. D'Auria, S. Starrfield, W. J. Thompson and M. Wiescher, *Astrophys. J. Suppl. Ser.* 134 151 (2001).
- [3] G. Audi, A. H. Wapstra and C. Thibault, *Nucl. Phys. A* 729 337 (2003).
- [4] R. A. Paddock, *Phys. Rev. C* 5 485 (1972).
- [5] J. M. G. Carança, R. D. Gill, A. J. Cox and H. J. Rose, *Nucl. Phys. A* 193 1 (1972).
- [6] E. Kuhlmann, W. Albercht and A. Hoffmann, *Nucl. Phys. A* 213 82 (1973).
- [7] H. Yokata, K. Fujioka, K. Ichimaru, Y. Mihara and R. Chiba, *Nucl. Phys. A* 383 298 (1982).
- [8] H. O. U. Fynbo *et al.*, *Nucl. Phys. A* 677 38 (2000).
- [9] D. W. Bardayan *et al.*, *Phys. Rev. C* 76 045803 (2007).
- [10] K. Setoodehnia *et al.*, *Nucl. Phys. A* 834 205c (2010).

2.2 Measurement of nuclear magnetic moment of unstable nucleus ^{40}Sc . II

Y.Ishibashi, A.Ozawa, T.Nagatomo¹, Y.Tagishi, Y.Abe, Y.Ito, H.Oishi, N.Kamiguchi, H.Suzuki, D.Nagae, T.Moriguchi and K.Matsuta²

The unstable nucleus ^{40}Sc ($I^\pi=4^-$, $T_{1/2}=182\text{ms}$) is located near stable nucleus ^{40}Ca , which is a doubly closed shell nucleus. Thus, its nuclear structure is interesting. However, the nuclear magnetic moment (μ) of ^{40}Sc has never been measured. Since μ is sensitive to the configuration mixing in the nucleus, we started the measurement of ^{40}Sc from the last year.

Last year, we measured only μ of ^{40}Sc in CaF_2 crystal. But we did not get the central value of μ of ^{40}Sc [1]. So, we did three improvements. First, we measured μ of ^{20}F in CaF_2 crystal for the system check. Production of polarized ^{20}F by polarized deuteron beam was performed at UTTAC previously [2]. Second, we changed β -NMR system to improve signal-to-noise ratio (S/N ratio). Therefore, to the previous system we added thick scintillation counters (10mm thickness) for measurement of energy spectrum of β -ray, and changed chamber material from Al to Delrin, as shown in Fig.1. At last we changed target from CaF_2 to CaO . Because μ of ^{41}Sc ($I^\pi=7/2^-$, $T_{1/2}=0.59\text{s}$) has been measured in CaO crystal [3], so we can expect that nuclear polarization of ^{40}Sc is maintained during its half-life. We made CaO target at RIKEN. First we made CaCO_3 pellet from CaCO_3 powder. Next, the pellet was put into oven, and baked at 900°C through one night. As a result, CaO is made from CaCO_3 .

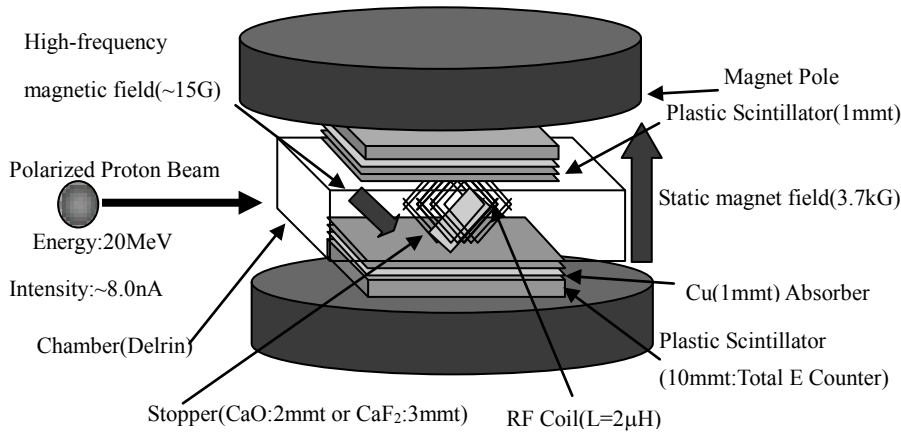


Fig.1 Experimental setup for β -NMR

Fig.2 shows time spectrum at three conditions. Time spectra in previous works are shown Fig.2(a), time spectra measured by new chamber is shown Fig.2(b), and time spectra measured in CaO target is shown Fig.2(c). From these figures, we calculated purity of ^{40}Sc at condition (a), (b), and (c), respectively, $60\pm 2\%$, $72\pm 1\%$, and $76\pm 1\%$. So we recognized that condition (c) is best and determined to measure in CaO target in future.

Fig.3 shows NMR spectrum of ^{20}F . Red (green) points are data that beam polarization direction is up (down), respectively. The central value of g-factor is 1.047, which is known value[4], and we observed

¹ International Christian University, Osawa 3-10-2, Mitaka, Tokyo 181-8585, Japan,

² Department of Physics, Osaka University, Toyonaka, Osaka 560-0043, Japan

nuclear polarization here. Furthermore, in Fig.3, nuclear polarization of ^{20}F was reversed when the direction of deuteron polarization was reversed. Thus, our detection system for β -NMR works properly.

Fig.4 shows NMR spectrum of ^{40}Sc . Red (green) points are data measured by CaO (CaF₂) target, respectively. From this figure, μ of ^{40}Sc has not been determined in both targets. We applied magnetic field=3.7kG in this time, but it may not be enough. Measurements at higher magnetic field are required for future experiments.

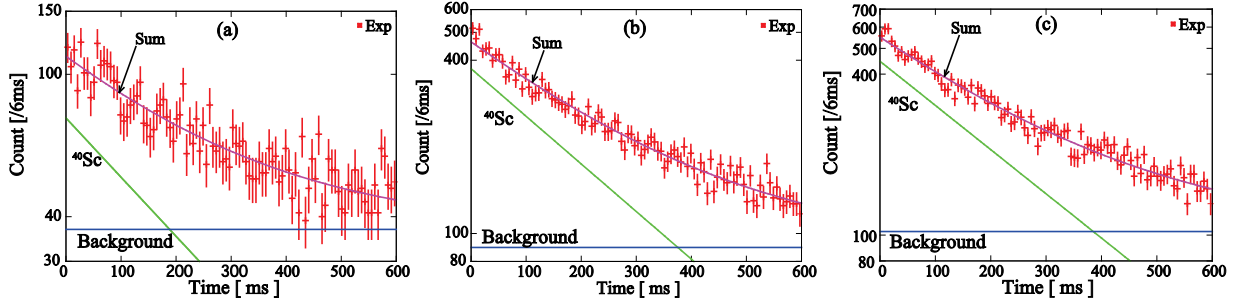


Fig.2(a) Time spectra measured in CaF₂ at old chamber (aluminum). (b) Time spectra measured in CaF₂ at new chamber (delrin). (c) Time spectra measured in CaO at new chamber (delrin).

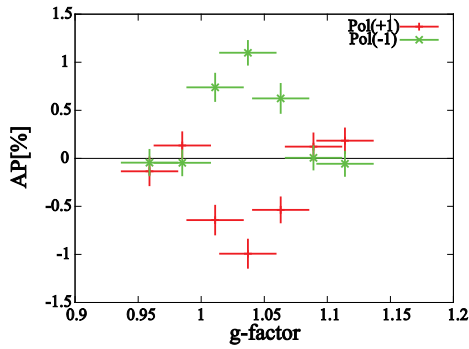


Fig.3 NMR spectrum of ^{20}F

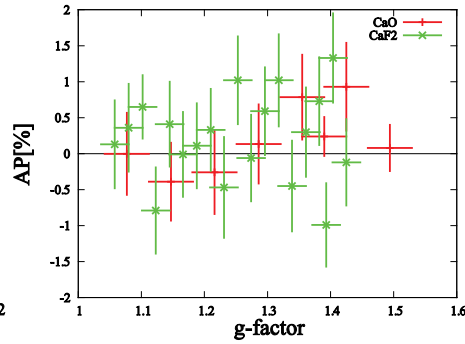


Fig.4 NMR spectrum of ^{40}Sc

Acknowledgement

The authors wish to thank the technical staffs of UTTAC for their supports during the experiment. We would like to thank Dr. Y. Kobayashi (RIKEN) for helpful make CaO target.

References

- [1] Y.Ishibashi et al., UTTAC ANNUAL REPORT 2008(2009)11
- [2] K.Matsuta et al., UTTAC ANNUAL REPORT 2004(2005)14
- [3] T.Minamisono et al., Nucl. Phys. A516(1990)365
- [4] N.J.Stone, Atomic Data and Nuclear Data Tables 90(2005)75

2.3 Measurement of nuclear magnetic moment of unstable nucleus ^{30}P

Y.Abe, A.Ozawa, H.Suzuki, Y.Tagishi, Y.Ishibashi, Y.Ito, H.Ooishi, D.Nagae, T.Moriguchi, K.Yokoyama, T.Nagatomo¹

The magnetic moments of the nuclei are suitable to investigate the nuclear structure. The unstable nucleus ^{30}P (half life $T_{1/2}=2.498$ min, $I^\pi=1^+$) is the self-conjugate nucleus, where the isospin is zero. The nuclear magnetic moment of ^{30}P has not been measured. We measured yield and purity of ^{30}P to optimize the beam condition.

The unstable nucleus ^{30}P were produced through the $^{30}\text{Si}(p,n)^{30}\text{P}$ or $^{29}\text{Si}(d,n)^{30}\text{P}$ reaction initiated by the beam of proton or deuteron obtained by 12UD Pelletron at Tandem Accelerator Complex, University of Tsukuba. A 8,9,10 MeV proton beam and 4,5 MeV deuteron beam irradiated natural Si ($^{28}\text{Si}:^{29}\text{Si}:^{30}\text{Si} = 92.23\%:4.67\%:3.10\%$) target. The intensity of proton beam was ~ 6 nA, deuteron beam was ~ 5 nA. The target was single crystalline Si 1.0 mm thick. All the ^{30}P nuclei were stopped in the same Si target. The β rays from the ^{30}P nuclei in the target were detected by two sets of plastic scintillation counters located above and below the target. These counters consisted of two plastic scintillators with a thickness of 1.0 mm.

A typical time spectrum of β rays is shown in Fig.1. The spectrum is fitted by two exponential functions. The ^{30}P nuclei was produced, however ^{29}P ($T_{1/2} = 4.142$ s, $I^\pi=1/2^+$) nuclei was also produced. We calculated a value of Figure of Merit (FOM), that is defined by $FOM = YP^2$, where Y is yield, P is purity. FOM should be as large as possible. Table 1 shows FOM for all experiment conditions. The best

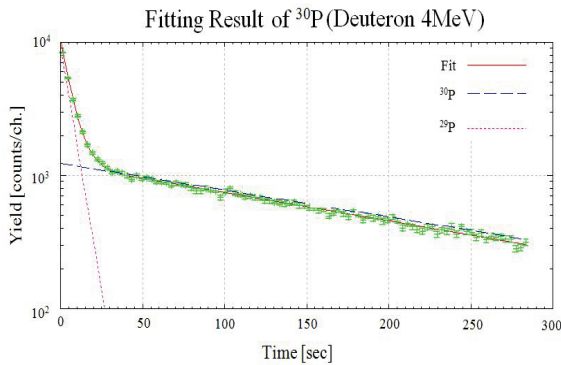


Fig.1. Typical time spectrum of ^{30}P and ^{29}P .

Table 1. The result of all experimental conditions.

Beam	Energy[MeV]	Yield[Count/sec]	Purity[%]	Figure of Merit
Proton	10	$(75.7 \pm 1.1) \times 10^3$	90.2 ± 0.1	$(61.6 \pm 1.0) \times 10^3$
Proton	9	$(66.2 \pm 1.0) \times 10^3$	93.1 ± 0.3	$(57.4 \pm 0.9) \times 10^3$
Proton	8	$(76.5 \pm 3.1) \times 10^2$	94.8 ± 0.3	$(68.8 \pm 3.0) \times 10^2$
Deuteron	5	$(91.8 \pm 1.6) \times 10^3$	80.6 ± 0.1	$(59.7 \pm 1.3) \times 10^3$
Deuteron	4	$(12.8 \pm 0.5) \times 10^4$	78.6 ± 0.1	$(79.2 \pm 1.2) \times 10^3$

¹ International Christian University, Mitaka, Tokyo, Japan

condition was a 4 MeV deuteron beam experiment.

We measured the magnetic moment of ^{29}P by the β -NMR method to check a polarization and measurement system [1]. It is already known as $\mu=1.2349(3)\mu_N$ [2].

The polarized ^{29}P was produced through the $^{29}\text{Si}(\vec{d},n)^{30}\text{P}$ reaction initiated by the polarized deuteron beam ($P=75\%$). A 4 MeV deuteron beam irradiated natural Si target. The intensity of polarized deuteron beam was ~ 2.5 nA. The target was single crystalline Si with 0.5 mm thickness. All ^{29}P nuclei were stopped in the same Si target. The β rays from the ^{29}P nuclei in the target were detected by three sets of plastic scintillation counter located above and below the target, where one set of plastic scintillation counters with a thickness of 10 mm were added. To keep nuclear polarization of ^{29}P inside the target, a static magnetic field H_0 (~ 1.9 kG and ~ 3.7 kG) was applied. To perform NMR, a radio-frequency (RF) magnetic field H_1 (~ 3.55 MHz and ~ 6.95 MHz) was applied by a Helmholtz coil.

We measured NMR spectra with two conditions. Observed NMR spectra are shown in Fig.2 and Fig.3. AP shown in Fig.3 is larger than AP shown in Fig.2, where A is asymmetry parameter of β -rays, P is polarization. Thus, the static magnetic field should be raised as much as possible. We will develop the system which can supply higher static magnetic field. After the development, we will perform the magnetic moment measurement of ^{30}P .

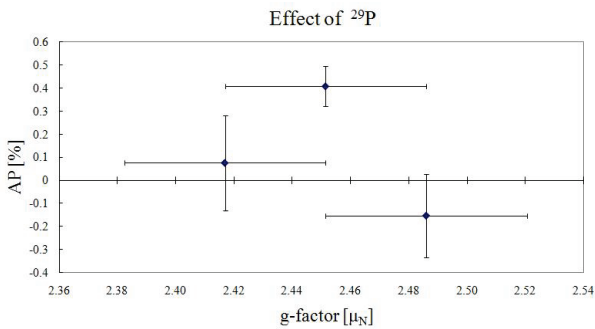


Fig.2. NMR spectrum in the case of $H_0=1.9$ kG.

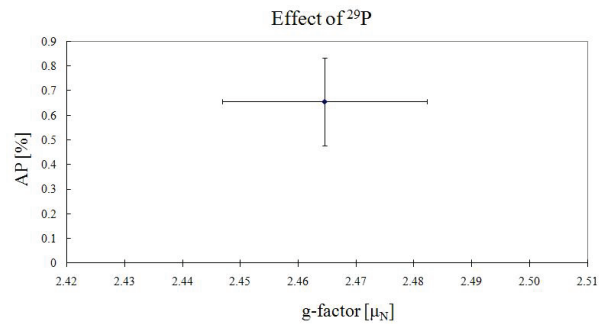


Fig.3. NMR spectrum in the case of $H_0=3.7$ kG

References

- [1] C.P. Slichter, Principles of magnetic resonance, 3rd enlarged and updated ed.
- [2] N.J. Stone, Atomic Data and Nuclear Data Tables 90 (2005) 75-176

2.4 Study of nuclear synthesis of ^{26}Al by gamma ray spectroscopy III

T. Komatsubara, Y. Sugiyama, A. Ozawa, Y. Abe, N. Kamiguchi, K. Yokoyama, T. Shizuma*, T. Hayakawa*, S. Kubono[#]

* JAEA

[#] CNS, Tokyo University

Since observation of 1.809-MeV gamma rays by satellite gamma ray telescope has been reported[1], the astrophysical study of ^{26}Al is very important for nuclear synthesis. Half life of the ^{26}Al is 7.2×10^5 year. The nucleus ^{26}Al can be created by $^{25}\text{Mg}(p,\gamma)$ reaction. However there is bypass reaction sequence $^{25}\text{Al}(p,\gamma)^{26}\text{Si}(\beta,\nu)^{26\text{m}}\text{Al}(\beta,\nu)$ which emits no gamma ray of 1.809-MeV. The excited states of ^{26}Si , key nucleus, have been studied by reaction mechanism[2-5] and gamma ray spectroscopy[6]. In our previous studies, one new level is found above proton threshold at 5886-keV in the ^{26}Si [7]. For the determination of spin of the observed state, gamma-ray angular correlation measurements were carried out[8].

In order to investigate the level structure in ^{26}Si , in-beam gamma ray spectroscopy was performed at UTTAC. The excited states of ^{26}Si were populated by the nuclear reaction $^{24}\text{Mg}(^3\text{He},n)^{26}\text{Si}$. The ^3He beam of 10 MeV was irradiated on a natural Mg target. Target thickness of the Mg foil is 3 mg/cm^2 . Gamma-gamma coincidence measurements were performed by using Ge detectors. Relative efficiencies of the Ge detectors are 40% and 35% at 1333-keV. In the previous angular correlation measurement, there was a uncertain parameter of normalization which used for correction of different solid angles of the detectors. In order to conserve the solid angles of the Ge detectors a goniometer of 1.5 m in diameter was newly installed in the present study. For the measurement of the DCO ratio [9], one detector is fixed at 90 degree and other is mounted on the turn table of the goniometer to move between 90 and 135 degree with respect to the beam axis.

As the results of the DCO measurement, the ratios are shown as crosses in Fig. 1 as a function of the gamma ray energy. The gate gamma ray is 1797-keV $2^+ \rightarrow 0^+$ transition. In this figure, previous results are shown as closed circles, and theoretical expectation values are also shown as open triangles.

For the 989-, 1537-, 1960-, and 2340-keV transitions, newly measured values are consistent to the previous results. Statistical error of the 2646-keV transition is quite large for the new result. For the 3875- and 4089-keV, DCO ratio can not evaluated in the new measurement because of the small efficiencies of the Ge detectors.

Because the new results with goniometer are rather consistent with previous results, evaluation of the normalization factor for the previous measurement is confirmed.

References

[1] R. Diehl, H. Halloin, K. Kretschmer, G.G. Lichti, V. Schönfelder, A.W. Strong, A. Kienlin, W. Wang, P. Jean, J. Knödseder, J.P. Roques, G. Weidenspointner, S. Schanne, D.H. Hartmann, C. Winkler, C.

Wunderer, Nature 439 (2006) 45.

[2] D.W. Bardayan, J.C. Blackmon, A.E. Champagne, A.K. Dummer, T. Davinson, U. Greife, D. Hill, C. Iliadis, B.A. Johnson, R.L. Kozub, C.S. Lee, M.S. Smith, P.J. Woods, Phys. Rev. C 65 (2002) 032801(R).

[3] J.A. Caggiano, W.B. Smith, R. Lewis, P.D. Parker, D.W. Visser, J.P. Greene, K.E. Rehm, D.W. Bardayan, A.E. Champagne, Phys. Rev. C 65 (2002) 055801.

[4] Y. Parpottas, S. M. Grimes, S. Al-Quraishi, C.R. Brune, T.N. Massey, J.E. Oldendick, A. Salas, T. Wheeler, Phys. Rev. C 70 (2004) 065805.

[5] P.N. Replowski, L.T. Baby, I. Wiedenhöver, S.E. Dekat, E. Diffenderfer, D.L. Gay, O. Grubor-Urosevic, P. Höflich, R.A. Kaye, N. Keeley, A. Rojas, A. Volya, Phys. Rev. C 79 (2009) 032801(R).

[6] D. Seweryniak, P.J. Woods, M.P. Carpenter, T. Davinson, R.V.F. Janssens, D.G. Jenkins, T. Lauritsen, C.J. Lister, J. Shergur, S. Sinha, A. Woehr, Phys. Rev. C 75 (2007) 062801(R).

[7] T. Komatsubara, K. Ebisu, T. Kawamata, A. Ozawa, K. Hara, T. Moriguchi, Y. Hashizume, T. Shizuma, T. Hayakawa, S. Kubono, UTTAC Annual Report 2007, UTTAC-77 (2008) pp. 15-16.

[8] T. Komatsubara, A. Ozawa, K. Hara, T. Moriguchi, Y. Ito, H. Satake, H. Ooishi, Y. Ishibashi, T. Shizuma, T. Hayakawa, S. Kubono, S. Hayakawa, D.N. Binh, A. Chen, J. Chen, UTTAC Annual Report 2008, UTTAC-78 (2009) pp. 13-14

[9] K.S. Krane, R.M. Steffen, R.M. Wheeler, Nuclear Data Tables, 11, (1973) 351.

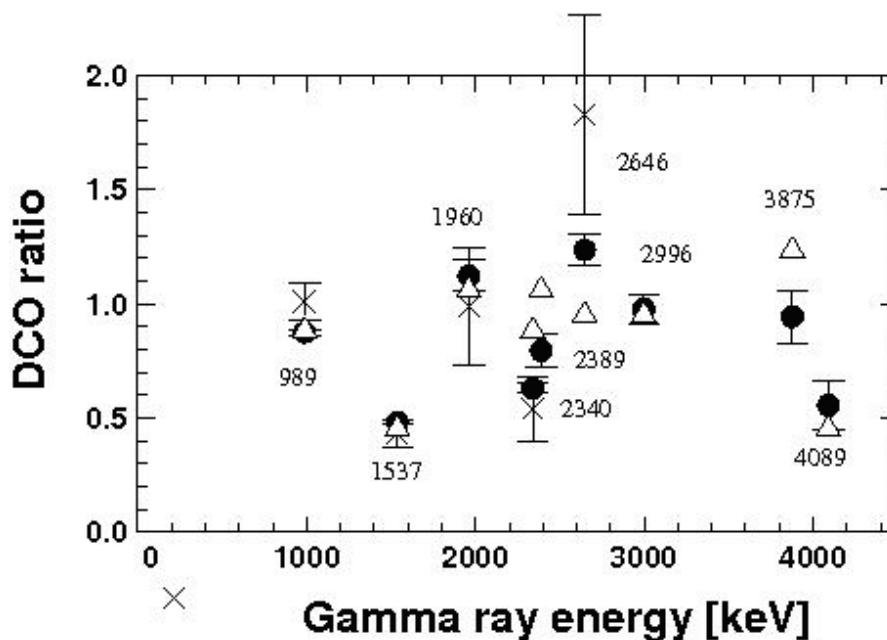


Fig.1 DCO ratios for ^{26}Si .

3.

MATERIALS AND CLUSTER SCIENCE

3.1 Electron emission from surfaces bombarded by MeV atom clusters

H. Kudo, H. Arai, S. Tomita, S. Ishii, and T. Kaneko¹

Pronounced suppression of electron emission from surfaces bombarded by fast clusters is one of the well known vicinage effects [1]. However, the main mechanism of the suppression still remains unsolved. We report on the recent analysis of the experimental data obtained at Tsukuba [2, 3], from which we conclude that the interference of wake potentials generated by the cluster atoms disturbs the escape of electrons, which gives rise to the observed suppression of electron emission [4, 5].

Figure 1 shows the energy spectra of low-energy electrons emitted from KCl(001) and highly-oriented pyrolytic graphite (HOPG) which were bombarded by C_n^+ beams of 12.5 keV/u (0.15 MeV/atom). For a measured energy spectrum, the integrated yield Y_n per n -atom cluster is given by the area under the spectrum, taking into account the energy dependence of the energy acceptance. Figure 2 shows the Y_n/Y_1 vs. n plots obtained from the present experiments for HOPG and KCl targets, where we see the typical linear n dependence. Similar results have been obtained also for 41.7 keV/u C_n . The observed values of the slope α (see Fig. 2) lie in the range $0.2 < \alpha < 0.4$.

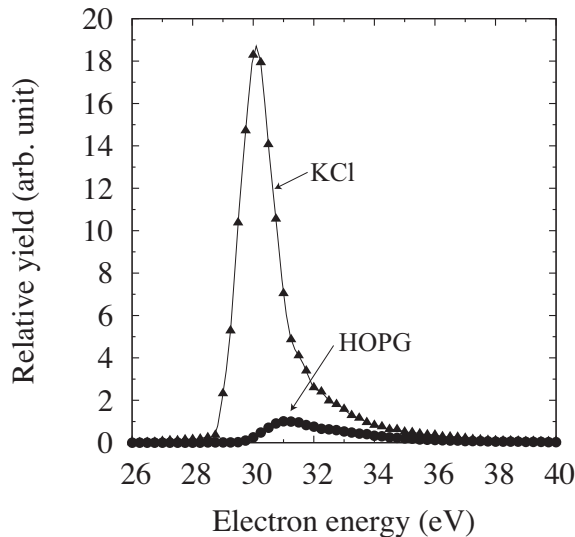


Fig. 1. Energy spectra of electrons emitted from KCl and HOPG bombarded by C_1^+ of 12.5 keV/u (0.15 MeV/atom). Note that the real zero-energy corresponds to 30 eV on the horizontal axis. The yields are shown for the same number of incident C atoms.

The observed n dependences of Y_n/Y_1 for KCl and HOPG are very similar, although Y_1 for KCl is higher than for HOPG by a factor of ~ 10 (Fig.1). Also, the difference between the two targets is much smaller than that in the case of suppression from $Y_n/Y_1 = n$. These results provide clear evidence against the possible effects associated with the surface transmission of electrons, nor with the track potential.

From the analysis of the linear n dependence of electron yield, we have specified the possible mechanism of suppressed electron emission from surfaces bombarded by fast clusters. Actually, the suppressed electron emission for cluster bombardment is predominantly caused by the disturbance of the electron

¹Okayama University of Science

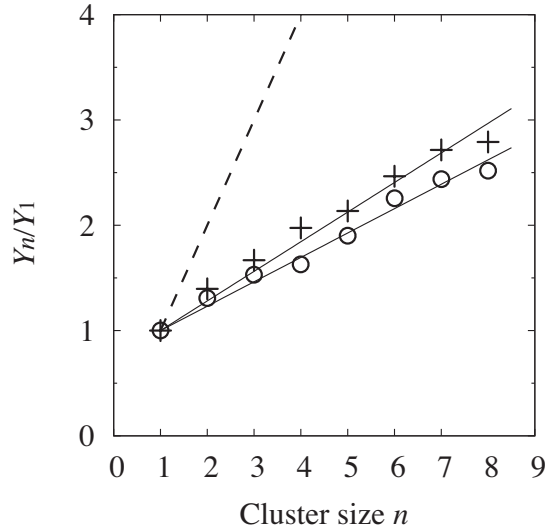


Fig. 2. Y_n/Y_1 values for impact of 12.5 keV/u C_n on HOPG and KCl targets. Circles and crosses show the yields for KCl and HOPG, respectively. The solid lines were drawn to determine the slope α , while the dashed line represents $Y_n/Y_1 = n$, i.e., absence of the vicinage effect.

escape due to the electric potential generated by moving cluster atoms. This model accounts for the observed n dependence of electron emission, and long-range interaction of dissociated cluster atoms in the electron transport process.

There is a possibility that the interference term, which appears in the expression of wake potential [6], gives rise to a shift from suppressed emission to enhanced emission of electrons as cluster speed increases, corresponding to that in the case of cluster stopping power. However, the applicability of the present model to enhanced electron emission for fast clusters in a Bethe stopping region requires careful further study.

References

- [1] See, for example, a review by M. Fallavier: Nucl. Instr. and Meth. B **112** (1996) 72.
- [2] H. Kudo, W. Iwazaki, R. Uchiyama, S. Tomita, K. Shima, K. Sasa, S. Ishii, K. Narumi, H. Naramoto, Y. Satoh, S. Yamamoto, T. Kaneko: Jpn. J. Appl. Phys. **45** (2006) L565.
- [3] S. Tomita, S. Yoda, R. Uchiyama, S. Ishii, K. Sasa, T. Kaneko and H. Kudo: Phys. Rev. A **73** (2006) 060901(R).
- [4] H. Arai, H. Kudo, S. Tomita, and S. Ishii, J. Phys. Soc. Jpn., **78** (2009) 104301.
- [5] H. Kudo, H. Arai, S. Tomita, S. Ishii, and T. Kaneko, Vacuum **84** (2010) 1014
- [6] T. Kaneko: Phys. Rev. A **66** (2002) 052991.

3.2 X-ray absorption spectroscopy of Mg-Ni and Mg-Ti hydride

D. Sekiba, K. Shiba, Y. Watahiki

Introduction

The Mg-based alloys, such as Mg-Ni, Mg-Ti, Mg-Fe etc., have attracted much attention as typical materials for the purpose of hydrogen storage. In order to develop the better hydrogen storage materials, the understanding of their electronic structures is important. So many experimental [1,2] and theoretical [3-5] efforts have been devoted to this field. Interestingly these Mg-based alloys show the metal-insulator transition by absorbing hydrogen. For example, the thin Mg₂Ni film (50 nm) deposited on a glass substrate is reflective metal, while Mg₂NiH₄ is reddish transparent semiconductor. However the mechanism of this metal-insulator transition has not been elucidated in terms of the electronic structure. We have been trying the in-situ X-ray absorption spectroscopy (XAFS) of Mg₂Ni and Mg₂Ti thin film in air and also hydrogen atmosphere.

Experimentals

The Mg₂Ni and Mg₂Ti film (200 nm thick) were deposited on the both sides of kapton films of 125 μm thick. The films were capped by 5 nm thick Pd layer to avoid the oxidation and enhance the dissociation of hydrogen molecules. For the deposition we used DC magnetron sputtering system in MANA foundry in National Institute for Materials Science. The exact compositions of the prepared alloys were determined by Rutherford back scattering (RBS) at the C-course of Tandatron accelerator in UTTAC. We newly designed a sample holder suitable to the hard X-ray absorption spectroscopy with the fluorescent mode in the hydrogen atmosphere (see Fig. 1). The both X-ray-absorption near-edge structure (XANES) and Extended X-ray-absorption fine structure (EXAFS) were measured at BL7C in Photon Factory in KEK.

Results and Conclusion

Figure 2 shows the XANES spectra taken at the Ni K-edge on the Pd/Mg₂Ni/kapton film. The black line indicates the initial state before the hydrogenation. We can see the shoulder-like features at 8316.5 and 8322.5 eV and a peak at 8340.8 eV. These spectral features are consistent with the previous report [1] taken by transmission mode and total fluorescence yield mode. After the dosage of Ar 98 % + H₂ 2 % gas with the pressure of 0.15 MPa in the newly made sample holder, the spectrum changed slightly (red line). The edge position shifted toward the higher photon energy. However this shift is much smaller compared with that reported in the previous paper [1]. We changed the sample gas to the pure H₂, then we obtained the spectrum plotted by green line. There we observed the edge shift with ~ 1 eV and the peak at 8340.8 eV remained at the same energy. These are consistent with the previous results. Thus it was confirmed the verification of our new sample holder and the sample preparation methods. As a next step, we applied the same method for the Mg-Ti alloys, for which no comprehensive study of XAFS have been made.

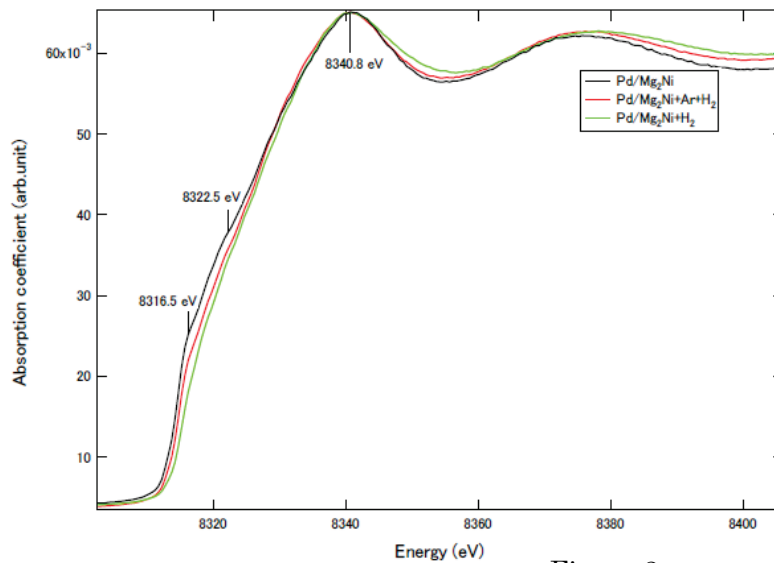
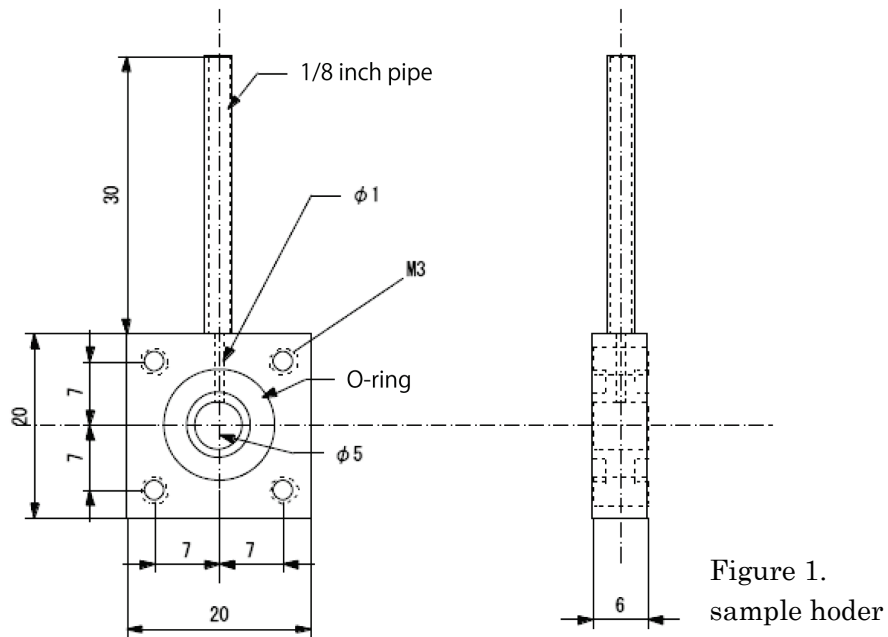


Figure 2.
XANES spectra on Mg-Ni

- [1] B. Farangis, P. Nachimuthu, T.J. Richardson, J.L. Slack, R.C.C. Perera, E.M. Gullikson, D.W. Lindle, M. Rubin, Phys. Rev. B 67 (2003) 085106.
- [2] M. Di Vece, A.M.J. van der Eerden, D. Grandjean, R.J. Westerwaal, W. Lohstroh, S.G. Nikitenko, J.J. Kelly, D.C. Koningsberger, Materials Chemistry and Physics 91 (2005) 1.
- [3] W.R. Myers, L-W. Wang, T.J. Richardson, M.D. Rubin, J. Appl. Phys. 91 (2002) 4879.
- [4] G.N. Garcia, J.P. Abriata, J.O. Sofo, Phys. Rev. B 59 (1999) 11746
- [5] Michiel J. van Setten, Gilles A. de Wijs, Phys. Rev. B 76 (2007) 075125.

3.3 The vicinage effect on energy loss of C_2^+ in a thin carbon foil.

S. Tamura, S. Tomita, Y. Narita, H. Tanikawa, K. Kurita, S. Isii, K. Sasa, and H. Kudo

When swift molecular ions are injected on a thin carbon foil, the energy loss of constituent individual atoms differ from the case of mono atomic ion injection. This effect is known as one of the vicinage effects, which was first reported by Brandt *et al.* [1] in 1974. Since then, many experimental results were reported for carbon clusters [2-4]. For an injection energy higher than 2.0 MeV/atom, it is shown that the vicinage effect is constructive, namely, the energy loss per atom for cluster ions is larger than that of an atomic ion ($\Delta E(C_n^+)/n > \Delta E(C^+)$). The results can be reproduced with the calculations based on the interference of response of the target electrons [5, 6]. However, in the low energy region below 1 MeV/atom, Kaneko [5] predicted the destructive effect while Heredia-Avalos *et al.* [6] reported constructive effect in the calculations. For the low kinetic energy below 1 MeV/atom, there have been only two reports so far [3, 4]. The experimental results reported by Brunelle *et al.* [3] show the destructive effect while Tomaschko *et al.* [4] show slightly constructive trend. In both cases, the uncertainty is too large to discuss such a small effect. In the present report, we performed the precise measurements of energy loss of C_2^+ in a thin carbon foil in the energy range from 0.33 to 0.66 MeV/atom.

Schematic drawing of the experimental setup is shown in Fig.1. The thin carbon foil whose thickness is $3.3 \mu\text{g}/\text{cm}^2$ was mounted on a mechanical system together with empty frame, which moved periodically so that carbon molecular beam penetrated the thin carbon foil and empty frame alternatively. Subsequently, the energy of carbon atoms that elastically scattered by Au on a amorphous carbon foil were measured at 100° by an ion-implanted-silicon charged-particle detector. The measured energy is proportional to the incident energy on Au target so that the energy of carbon atoms after penetration through the thin carbon foil can be measured.

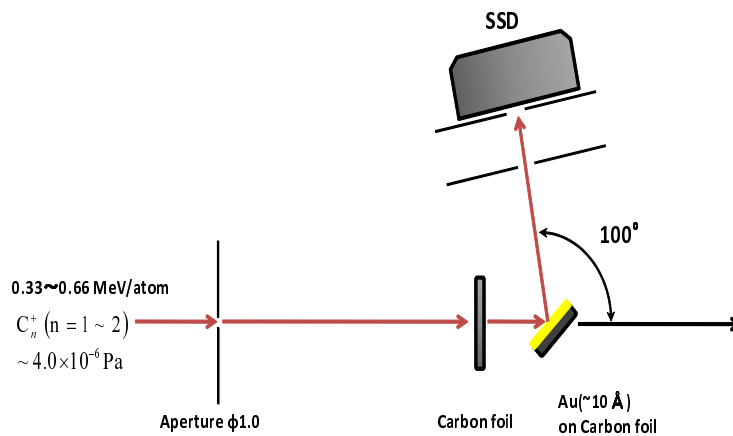


Fig. 1. Schematic drawing of the experimental setup.

The energy dependence of the difference between the energy loss of C_2^+ per atom and C_1^+ with same velocity is shown in Fig.2, together with all experimental results reported so far [2-4]. It is clearly seen that our error bar is extremely small compared to the other data. In the energy range from 0.33 to 0.66 MeV/atom, the energy loss of C_2^+ per atom is decreased 1 to 5 % compared to that of C_1^+ . The experimental values are in agreement with theoretical calculations [5]. The reversal of the effect seems to take place around the velocity of 1 MeV/atom for carbon cluster ions.

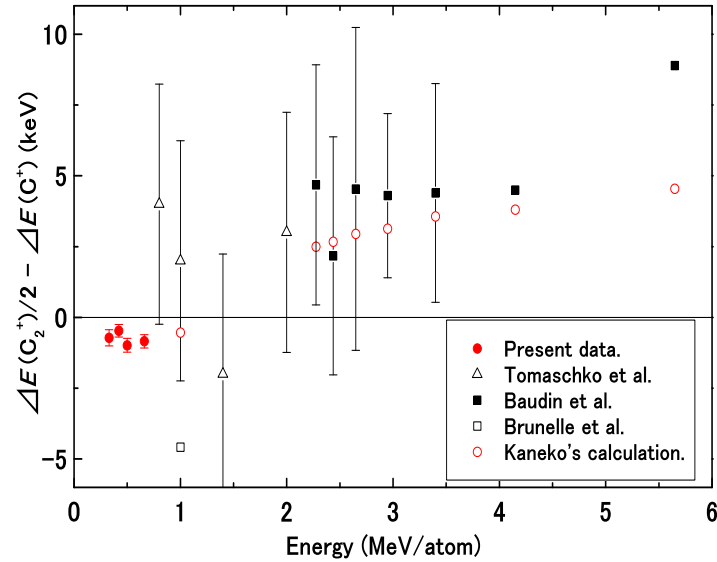


Fig. 2. The difference between the energy loss of C_2^+ per atom and C_1^+ with same velocity. Present results (filled circles), Baudin et al. (filled squares) [2], Brunelle et al. (open square) [3], Tomaschko et al. (open triangles) [4], Kaneko's calculation (open circles) [5].

References

- [1] W. Brandt, A. Ratowski, and R. H. Ritchie, *Physical Review Letters* 33, 1325 (1974).
- [2] K. Baudin, A. Brunelle, M. Chabot, S. Della-Negra, et al., *Nucl. Instrum. Methods Phys. Res. Section B* 94, 341 (1994).
- [3] A. Brunelle, S. Della-Negra, J. Depauw, D. Jacquet, Y. Le Beyec, and M. Pautrat, *Phys. Rev. A* 59, 4456 (1999).
- [4] C. Tomaschko, D. Brandl, R. Kügler, M. Schurr, and H. Voit, *Nucl. Instrum. Methods Phys. Res. Section B* 103, 407 (1995).
- [5] T. Kaneko, *Phys. Rev. A* 66, 052901 (2002).
- [6] S. Heredia-Avalos, R. Garcia-Molina, and I. Abril, *Phys. Res. A* 76, 012901 (2007).

3.4 Study on nitrogen diffusion in ϵ -Fe₂₋₃N submicron particles

M. Minagawa, H. Yanagihara, M. Kishimoto and E. Kita

Iron nitrides have been attracting much attention as magnetic materials because of their unique properties, such as large saturation magnetization, large magnetic anisotropy[1, 2] and high corrosion resistance. Additionally, their compound are only composed of non-rare elements and have high potentials as environmentally-enhancing materials being alternatives of current high performance magnetic materials including rare metals such as FePt and NdFeB.

Iron nitrides are categorized to be interstitial compounds and the crystal structure depends on the nitrogen content and magnetic properties also change. The typical iron nitride are α '-Fe₁₆N₂ (bct), γ '-Fe₄N (fcc) and ϵ -Fe₃N(hcp) that are ferromagnetic at room temperature.

The ϵ phase Iron nitrides are stable and the nitrogen concentration varies from 25 at.% to 33 at.% corresponding to the nitrogen concentration of x , $0 \leq x \leq 1$, for ϵ -Fe_{3-x}N. The phase posses superior corrosion and mechanical properties and were well studied.[3] The magnetic properties in the phase were reported to be largely influenced by the nitrogen concentration. Curie temperatures and magnetic moments decrease drastically with the increase of nitrogen concentration[4].

It is important for these nano-structured iron nitrides to elucidate fundamental properties in order to use as new types of magnetic materials. To clarify that fundamental physical and magnetic properties bulk samples are preferable, however bulk synthesized by usual methods will have a nitrogen concentration gradient. On the other hand, nano-sized particles can be crystallized in a single phase nitride much easier than bulk. Because they have a large surface area, nitrogen atoms can penetrate easily and uniformly into the particles. Extending the size of the particles with in single-phase, it is possible to make an accurate characterization with the small surface effects.

In this study, we used 180 nm Fe₃O₄ particles with relatively large size as starting material and synthesized single phase ϵ -Fe₂₋₃N. The use of large particles has an advantage that the influence of surface oxidization can be suppressed. By annealing in H₂ atmosphere, nitrogen concentrations were varied and were deduced from the lattice parameters. Nitrogen diffusion is discussed supposing the uniform distribution of nitrogen atoms in particles.

180 nm Fe₃O₄ particles were used as starting materials and were reduced in H₂ flow at 673 K to 2.5 h. Reduced samples were nitrided in NH₃ flow for 24 h at various temperatures. Then we obtained the optimum temperature at which single-phase ϵ -Fe₂₋₃N can be generated. The backward growth of the sample, decreasing the nitrogen concentration, was achieved by annealing the samples at 603 K in H₂ flow with varying annealing time. A usual backward growth procedure is done by the annealing in the gas mixture of NH₃ and H₂ at lower temperature than the nitriding temperature,[3] however, we used H₂ atmosphere. X-ray diffraction (XRD) was carried out for identification of resulted phase and determination of lattice constants.

Mössbauer spectra were recorded at room temperature. Data were numerically analyzed with a commercially available fitting software, MossWin ver.3. Samples for Mössbauer spectroscopy were sealed in plastic capsules with epoxy or vanish to prevent the oxidation.

Samples reduced from the Fe₃O₄ particles were confirmed to be in an α -Fe single phase. Nitrided

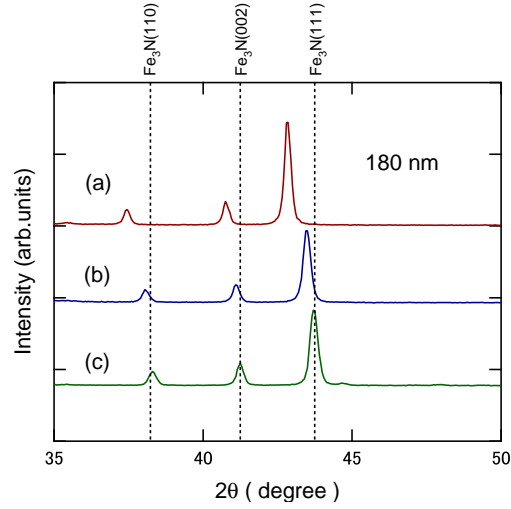


Fig. 1. XRD patterns of iron nitrides in diameters of 180 nm, as-nitrided sample (a), H₂ annealed sample at 603 K for 2 h (b) and H₂ annealed sample at 603 K for 4 h (c).

sample at temperatures around 623 K showed ϵ -Fe₂₋₃N single phase. Especially the sample nitrided at 623 K was sufficiently nitrided, therefore, the sample is labeled as "as-nitrided"(a). Figure 1 shows XRD patterns and the as-nitrided sample revealed to have the hcp structure with larger unit cell than that of bulk ϵ -Fe₃N. This result inferred the excess nitrogen atoms enlarged the lattice. Its lattice constants are $a = 0.480$ nm and $c = 0.443$ nm. Nitrogen concentration x in ϵ -Fe _{x} N was reported to have a relation between lattice constants of a hcp structure as follows,[4]

$$x = \frac{0.0673}{a - 0.44709} = \frac{0.0318}{c - 0.42723}. \quad (1)$$

Then x for the sample (a) was estimated to be 2.0 and nitrogen atoms are packed up to the limit of hcp structure. The sample annealed in H₂ flow for 2 h has lattice constants of $a = 0.473$ nm and $c = 0.439$ nm, and the chemical formula was ϵ -Fe_{2.6}N. The sample with 4 h annealing (c) had the lattice constants identical to the bulk ϵ -Fe₃N, $a = 0.470$ nm and $c = 0.438$ nm. Peaks in XRD shifted through the annealing, however, no line broadening was observed. This depicts that concentration gradient of nitrogen atoms in the particles did not occur and uniform distribution is realized.

Mössbauer spectra recorded at room temperature are shown in Fig.2 (A). The spectra for the as-nitrided sample (a) compose of two singlets, which indicates the sample was paramagnetic. The sample (b) with the H₂ anneal for 2 h revealed to be in a magnetically order state where the magnetic transition temperature is higher than room temperature. The spectrum was fit to a distributed Hyperfine field(H_{hf}) spectrum and the distribution histograms are shown in Fig. 2(B). The peak in H_{hf} was observed at around 20.8 T which coincides with that of ϵ -Fe_{2.6}N.[5]. There are two extra peaks at lower magnitude of H_{hf} indicating the distribution in magnetic transition temperature. The spectrum for the sample (c) was composed of two ferromagnetic sub-spectra. The major component has a distributed H_{hf} with a peak H_{hf} of 23.8 T. An additional ferromagnetic component about 5.4 % of area ratio was detected and the averaged hyperfine field is 29.9 T. It was also attributed to ϵ -Fe₃N[5].

Diffusion process of the ϵ phase particles was analyzed using data for samples with different nitrogen

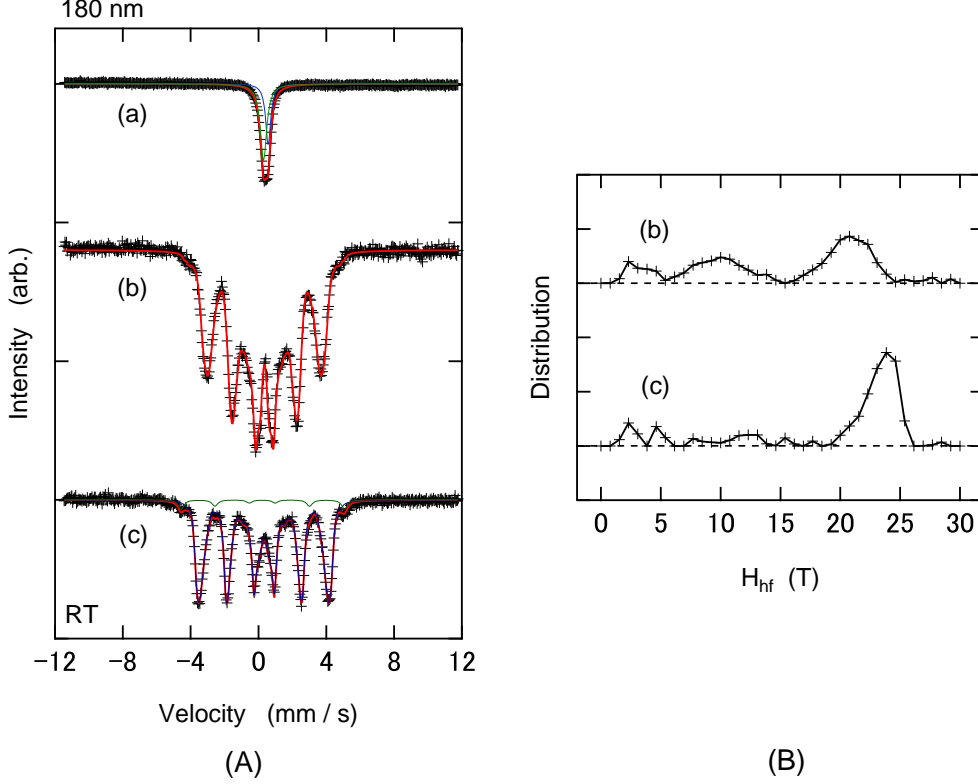


Fig. 2. (A) Mössbauer spectra for iron nitrides recorded at room temperature. Spectra for the as-nitrided (a), H₂ annealed for 2h (b), and H₂ annealed for 4h (c) samples are shown. Samples (a), (b) and (c) correspond to ϵ -Fe₂N, ϵ -Fe_{2.6}N and ϵ -Fe₃N. The distributions in hyperfine fields for samples (b) and (c) are displayed in panel (B).

concentration and the same crystalline structure. The diffusion in a sphere was expressed by the following equation,[6]

$$\frac{\bar{c} - c_e}{c_a - c_e} = \frac{6}{\pi^2} \exp\left(-\frac{\pi^2}{r_0^2} Dt\right). \quad (2)$$

Here, \bar{c} , c_e , c_a , D , are t are an average concentration, a surface concentration at the end, an initial concentration, a diffusion constant and a reaction time, respectively. We supposed $c_e = 0$, D because the backward diffusion was occurred in this case. The diffusion constant is therefore expressed as follows,

$$D = -\frac{r_0^2}{\pi^2 t} \ln \frac{\pi^2 \bar{c}}{6c_a}. \quad (3)$$

By the H₂ annealing for 4 h, nitrogen concentration decreased from 33 at.% to 25 at.%. Taking $c_a = 33$ at% and $\bar{c} = 25$ at%, the diffusion constant at 603 K was estimated to be $D = 6.33 \times 10^{-20}$ [m²/sec]. This is a diffusion constant of nitrogen in the hcp structure, D_{hcp} .

The diffusion constant of thin plate ϵ -Fe₂₋₃N was expressed as $D_N^\epsilon = 1.68 \times 10^{-7} \exp(-118000/RT)$ m²/sec[3]. From the relation, the bulk diffusion constant is found to be $D_N^\epsilon = 1.01 \times 10^{-17}$ m²/sec at 603 K. It is about three order larger than that obtained in the present work. The difference might be caused by the anti-sintering process at the particle surface suppressing the nitrogen diffusion. For reference, the diffusion constant of nitrogen in bcc α -Fe was expressed as $D = 4.88 \times 10^{-7} \exp(-76900/RT)$ m²/sec[6].

The value at 603 K is $D = 1.06 \times 10^{-13} \text{ m}^2/\text{sec}$. This shows that the diffusion constant in hcp is essentially smaller than that in the bcc phase.

The diffusion constants of nitrogen atom in the hcp phase Fe both in bulk and small particles are smaller than that in bcc phase. The difference may originate from the characteristics of the crystalline structure. The hcp and fcc structures belong to the closed pack structure and movement of the guest atoms among the interstitial sites has less probability than the case in the bcc (not closed packed) structure. It is interesting that the nitrogen diffusion constant is three order smaller than that in the bulk specimen. The smaller coefficient means that the nitrogen atoms do not move easily. Providing the two dimensional diffusion, nitrogen penetration depth, x , is expressed as the relation, $x^2 \propto D\tau$. [7] From the relation, the uniform nitrogen concentration range in the fine particles was roughly speculated to be $10^{-3/2} \simeq 0.03$ times smaller than that for the bulk. Supposing 10 μm of the uniform range in bulk, the nitrogen uniform range for fine particles is estimated to be 300 nm. This suggests the upper particle size of ϵ single phase particles.

This work was supported by a Grant-in-Aid Scientific Research (Grant No. 19560661) under MEXT, Japan.

References

- [1] Y. Sasaki, N. Usuki, K. Matsuo, and M. Kishimoto, IEEE Tran.Magn. 41, 3241 (2005).
- [2] E. Kita, K. Shibata, H. Yanagihara, Y. Sasaki, and M. Kishimoto, J. Magn. Magn. Mater. 310, 2411 (2007).
- [3] T. Liapina, A. Leineweber, and E. J. Mittemeijer, Metall. Mater. Trans. 37A, 319 (2006).
- [4] M. A. J. Somers, B. J. Kooi, L. Maldzinski, E. J. Mittemeijer, A. A. van der Horst, A. M. van der Kraan, and N. M. van der Pers, Acta Mater. 45, 2013 (1997)
- [5] M. Kopcewicz, J. Jagielski, A. Turos, and D. L. Williamson, J. Appl. Phys. 71, 4217 (1992).
- [6] T. Heumann, *Diffusionin Metallen* (Springer-Verlag, Berlin, 1992).
- [7] W. P. Tong, C. S. He, J. C. He, L. Zuo, N. R. Tao, and Z. B. Wang, Appl. Phys. Lett. 89, 021918 (2006).

4.

ACCELERATOR MASS SPECTROMETRY

4.1 Fluctuations in cosmic ray flux around 11 kyr BP based on cosmogenic ^{36}Cl from the Dome Fuji ice core

K. Sasa, K. Kurosumi, Y. Matsushi, Y. Tosaki, T. Takahashi, K. Sueki, N. Kinoshita, K. Horiuchi, H. Matsuzaki and H. Motoyama

Cosmogenic radionuclides such as ^{10}Be , ^{14}C and ^{36}Cl are produced in the Earth's atmosphere by the interaction of galactic cosmic rays with the atoms. The connection between cosmogenic radionuclide production and the geomagnetic field is well understood [1]. We reconstruct past changes in cosmic ray flux under the assumption that cosmogenic nuclide records are mainly influenced by changes in their production rates. Cosmic ray fluctuations around 11 kyr BP have already been observed in ^{14}C records from the analysis of ^{14}C tree ring and ^{10}Be data from the ice cores at Greenland [2]. We report the results of ^{36}Cl flux around 11 kyr BP from the ice core at the Dome Fuji station ($77^{\circ}19'01''\text{ S}$, $39^{\circ}42'12''\text{ E}$) in Antarctica [3].

Ice core samples were obtained from 370 m to 320 m below the surface of the ice sheet, corresponding to ages of 12.3–10.5 kyr BP. The record of ^{36}Cl flux increases between 11.4 and 11.2 kyr BP. The result agrees well with ^{14}C records derived from ^{14}C tree ring and ^{10}Be data measured from the Greenland ice cores. Cosmic ray fluctuations derived from the ^{36}Cl flux in the Dome Fuji ice core agree with independent geomagnetic field intensity reconstructions.

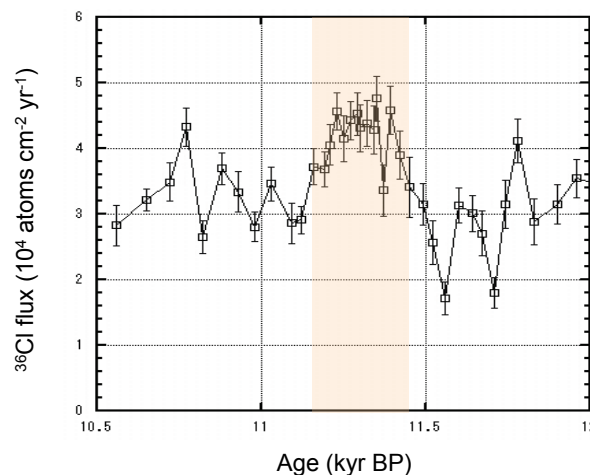


Fig. 1 ^{36}Cl flux around 11 kyr BP measured in the Dome Fuji ice core (Antarctica).

Acknowledgements

This work is supported in part by the Grants-in-Aid for Scientific Research Program of the Ministry of Education, Culture, Sports, Science and Technology, Japan.

References

- [1] J. Beer, R. Muscheler, G. Wagner, C. Laj, C. Kissel, P. W. Kubik, H-A. Synal, *Quaternary Science Reviews* 21 (2002) 1129-1139.
- [2] J. Masarik, J. Beer, *J. Geophys. Res.* 104/D10 (1999) 12099.
- [3] H. Motoyama, *Scientific Drilling* 5, (2007) 41–43.

4.2 Distribution of ^{36}Cl in the Yoro River basin and its relation to regional groundwater flow system

Y. Tosaki, N. Tase, K. Sasa, T. Takahashi and Y. Nagashima

Introduction

Understanding of groundwater flow system plays an important role in sustainable management of water resources. Application of environmental tracers is one of the effective approaches for visualizing the movement of groundwater. For the purpose of testing the potential of ^{36}Cl to trace regional groundwater flow system with a time scale of ~ 50 years, spatial distribution of ^{36}Cl was investigated in the lower reach of the Yoro River basin, Chiba Prefecture.

Study area and methods

The downstream area of the Yoro River is characterized by its surrounding Pleistocene uplands and alluvial lowlands along the river. The climate in this region is humid temperate, with an average annual precipitation of 1590.2 mm at Ushiku in the southern hilly area, and 1293.8 mm at Chiba, which is located on the northwestern side of the study area near the coast along Tokyo Bay.

A previous study clearly demonstrated the regional groundwater flow in the basin by using tritium as a tracer [1]. Recharge mainly occurs at upland areas, and the groundwater essentially flows into the lowland along the Yoro River eventually discharging into the river.

Groundwater samples were collected from 16 irrigation wells located within the basin (Fig. 1) in July and August, 2004, and analyzed for dissolved inorganic ions by ICP-AES and ion chromatography. After standard chemical processing [2], $^{36}\text{Cl}/\text{Cl}$ ratios were measured with the AMS system at UTTAC.

Results and discussion

Table 1 lists dissolved anion concentrations and ^{36}Cl data for the samples analyzed in this study. Samples I-2 and I-10 showed relatively high Cl^- concentration and high NO_3^- concentration as well, possibly affected by anthropogenic chlorine source. In order to minimize the possible mixing effect of artificial chloride, ^{36}Cl concentrations were used for data interpretation assuming a negligible content of ^{36}Cl in chloride derived from such artificial source.

Figure 2 shows the distribution of ^{36}Cl concentration projected onto the line A-B in Fig. 1. Although sample I-1 is located rather far from the projection line, it was also included as a value representing

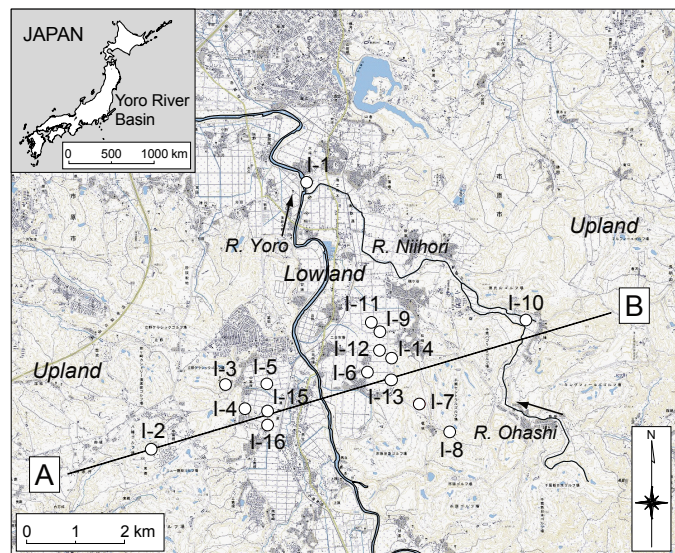


Figure 1. Location of the wells sampled in this study.

groundwater in the discharge area. Relatively low ^{36}Cl concentrations were only found in the lowland near the river, while the others showed higher values. The observed distribution is basically consistent with the groundwater flow system traced by environmental tritium in 1980s [1]: relatively young groundwater in the upland areas and old groundwater (>30 years) in the lowland. Low ^{36}Cl concentrations in the lowland suggest even longer residence times, probably more than 50 years. Our observation demonstrates that the distribution of ^{36}Cl is effective for tracing groundwater recharged during the last ~50 years.

Table 1
Anion concentrations and ^{36}Cl data for the groundwater samples in the Yoro River basin.

Sample	Depth (m)	Cl^- (mg/L)	NO_3^- (mg/L)	SO_4^{2-} (mg/L)	HCO_3^- (mg/L)	$^{36}\text{Cl}/\text{Cl}$ (10^{-15})	^{36}Cl (10^6 atoms/L)
I-1	48–60	6.3	0.2	4.0	143.4	25 ± 3	2.7 ± 0.3
I-2	10	19.9	93.3	0.1	6.1	61 ± 5	20.6 ± 1.8
I-3	14–27	11.8	0.8	29.3	163.5	140 ± 9	27.9 ± 1.8
I-4	24–27	7.8	0.3	7.1	142.7	150 ± 9	19.9 ± 1.2
I-5	n.k.	5.6	0.2	8.1	118.3	29 ± 20	2.8 ± 1.9
I-6	56–100	7.5	0.2	13.3	100.0	216 ± 13	27.5 ± 1.7
I-7	50–72	7.4	0.2	14.6	145.8	225 ± 15	28.2 ± 1.9
I-8	32–54	6.7	3.4	10.4	68.9	345 ± 17	39.4 ± 2.0
I-9	56–100	7.7	0.2	16.2	150.7	161 ± 14	21.2 ± 1.9
I-10	25	15.7	32.0	10.3	143.4	243 ± 18	65.1 ± 4.8
I-11	54–78	7.6	0.2	25.5	160.4	258 ± 11	33.2 ± 1.5
I-12	n.k.	7.0	0.3	10.6	111.0	65 ± 13	7.8 ± 1.6
I-13	95–150	7.0	0.2	15.8	103.7	362 ± 20	43.2 ± 2.4
I-14	56–100	7.1	2.2	15.1	133.6	128 ± 8	15.4 ± 1.0
I-15	80–105	6.0	0.2	8.2	151.3	17 ± 3	1.8 ± 0.3
I-16	18–32	11.6	0.2	2.7	280.6	117 ± 10	23.1 ± 2.0

n.k.: not known.

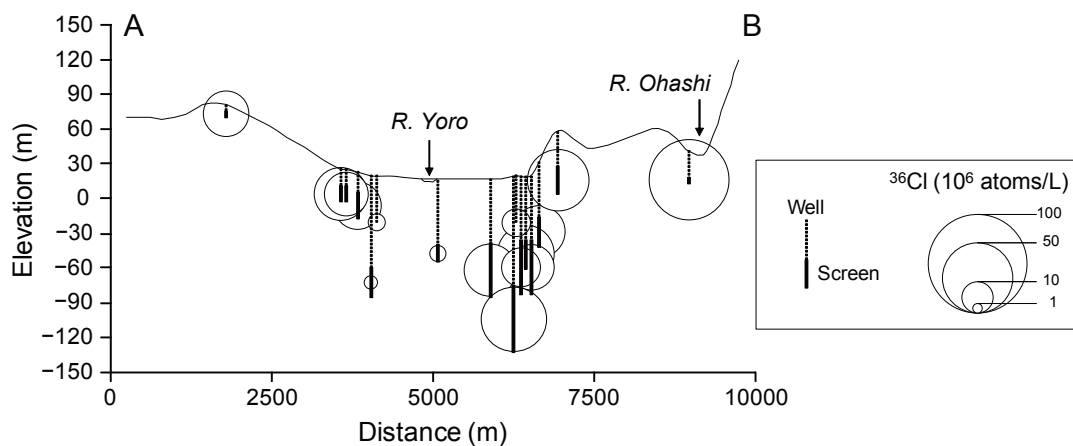


Figure 2. Cross-sectional distribution of ^{36}Cl concentration along the line A-B shown in Figure 1.

Reference

- [1] A. Kondoh, Geograph. Rev. Japan., 58 (1985) 168 (in Japanese with English abstract).
 [2] Y. Tosaki et al., Nucl. Instr. and Meth. B 259 (2007) 479.

4.3 Measurement of ^{36}Cl in soil : Study of extraction methods according to reservoirs

T. Amano, K. Sueki, J. Kitagawa, K. Sasa, Y. Nagashima, Y. Takaya, T. Takahashi, N. Kinoshita, Y. Tosaki, Y. Matsushi¹, K. Bessho², H. Matsumura²

Introduction

Chlorine-36 which is a long life radioisotope is mainly produced by a nuclear spallation reaction with cosmic-ray on ^{40}Ar in the upper atmosphere^[1]. The nuclide is distributed whole earth. The atmosphere also contains ^{36}Cl which is produced in atmospheric nuclear tests on the sea. ^{36}Cl in soil has important roles to search chlorine circulation. We have measured ^{36}Cl which was extracted with HNO_3 from soil. We examined sequential extraction methods for ^{36}Cl determination.

Experiments

We examined extraction process of soil sample as shown in Figure 1. Soil sample which was dried and mashed up was extracted with 0.01 mol / l HNO_3 . Precipitate of hydroxide was prepared by adding 3 mol / l NH_3 to extracted solution. The precipitate was removed by a centrifugation, and then AgCl was prepared (hereinafter “A”). After extraction, dried soil of 20 g was mixed with 70 ml of 0.02 mol / l HNO_3 and 70 ml of 30 % H_2O_2 . The extraction was carried out for 1 day, and then solution was separated from the soil by a centrifugation. AgCl from the solution was prepared (hereinafter “B”) after the same procedure described for “A”. After two times of extraction, the soil was heated at 700 °C for 4 hours to remove organic matters and then heated at 1000 °C for 2 hours. Generated gas was trapped in alkali solution which 8.5 g of NaOH and 0.85 g of Na_2SO_3 were dissolved in 170 ml of water. 5 ml of 30 % H_2O_2 was added to the alkali solution, and then AgCl was prepared (hereinafter “C”). In addition, the soil was heated at 1000 °C after extraction with 0.01 mol / l HNO_3 and AgCl was prepared (hereinafter “D”). Each AgCl sample was loaded to target cone for determination of $^{36}\text{Cl}/\text{Cl}$ isotopic ratio using an accelerator mass spectrometry at UTTAC^[2].

Results and discussion

Table 1 shows $^{36}\text{Cl}/\text{Cl}$ isotopic ratios and supply sources of Cl. Cl isotopes extracted in sample “A” is supplied from soil water, because Cl extracted in sample “A” is a soluble species in the diluted acid. Cl in sample “B” and “C” are isolated from organochlorine compounds and inorganic minerals, respectively. Cl in sample “D” is mixture of “B” and “C”. Not significant difference was found in $^{36}\text{Cl}/\text{Cl}$ isotopic ratios between “A” and “B”. $^{36}\text{Cl}/\text{Cl}$ isotopic ratio in sample “C” is higher than “A” and “B”. $^{36}\text{Cl}/\text{Cl}$ isotopic ratio in organic matter and soil water show similar ratio. However, $^{36}\text{Cl}/\text{Cl}$ isotopic ratio in inorganic minerals shows higher $^{36}\text{Cl}/\text{Cl}$ isotopic ratio.

¹ Micro Analysis Laboratory, Tandem accelerator, The University of Tokyo.

² Radiation Science Center, High Energy Accelerator Research Organization.

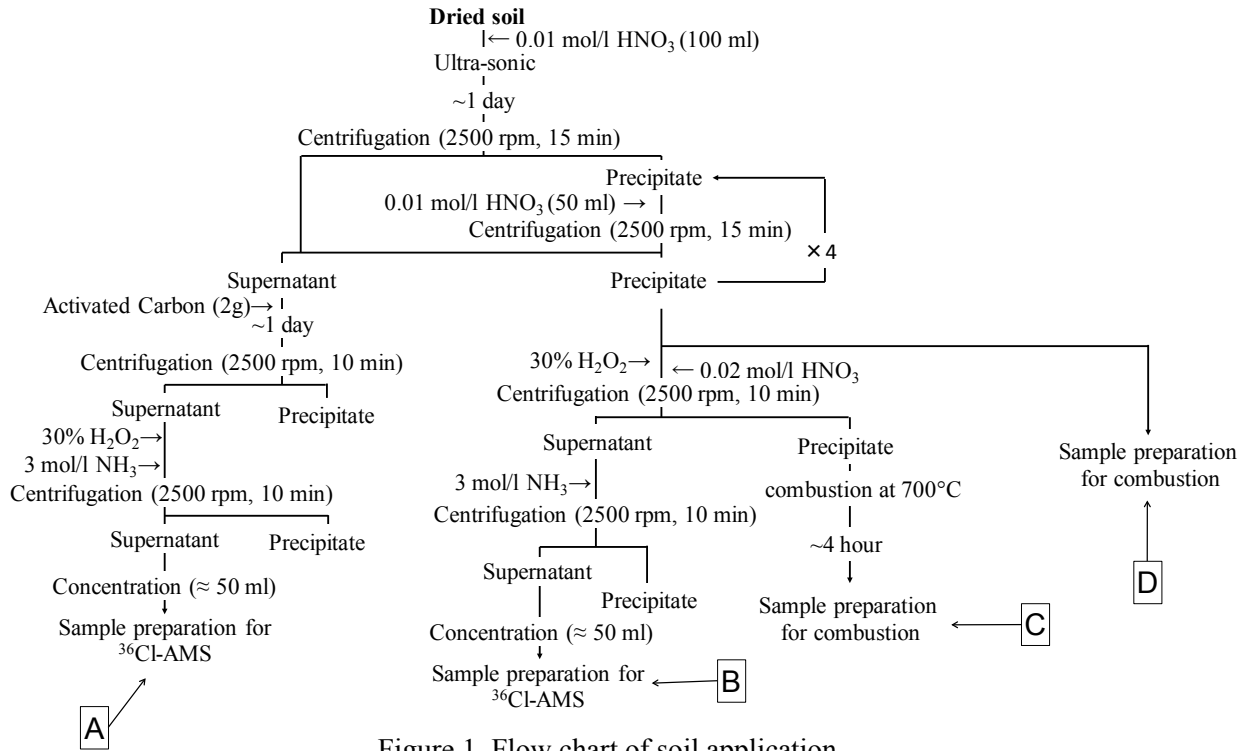


Figure 1. Flow chart of soil application

Table 1. The $^{36}\text{Cl}/\text{Cl}$ isotopic ratios and the supply source of chlorine in soil

Sample	$^{36}\text{Cl}/\text{Cl}$ ($\times 10^{-14}$)	Supply source of Cl
A	10.5±0.8	Soil water
B	11.5±0.7	Organic matters
C	14.3±0.6	Inorganic minerals
D	12.5±0.3	Mixture of B and C

References

- [1] H.-A. Synal, J. Beer, G. Bonani, M. Suter, and W. Wolfli, *Nucl. Inst. Meth. in Phys. Res. B*, **52** (1990) 483-488.
- [2] K. Sasa, Y. Nagashima, T. Takahashi, R. Seki, Y. Tosaki, K. Sueki, K. Bessho, H. Matsumura, T. Miura, and M. He, *Nucl. Inst. Meth. in Phys. Res. B*, **259** (2007) 41-46.

4.4 Chlorine-36 produced in muon irradiation

N. Kinoshita, K. Sasa, T. Takahashi, K. Sueki, Y. Tosaki, Y. Takaya, M. Matsumura, S. Abe, Y. Nagashima, T. Amano, K. Kurosumi, J. Kitagawa, Y. Matsushi¹, H. Matsumura², H. Iwase², Y. Kasugai², N. Matsuda², H. Yashima³, A. Leveling⁴, D. Boehnlein⁴, N. Mokhov⁴

The fast muon, decay product of pion, is one of secondary cosmic rays coming to surface Earth from upper atmosphere. Recently, the muon has been applied for imaging of volcanic structure [1]. In addition, the muon activates surface Earth's rock. The radioisotopes, which originate from muon, have been used for an estimation of erosion rate of surface rock [2]. There are several potentials for application using the muon. Thus, physical properties of the muon such as stopping power and nuclear reaction, are important for supporting the purposes.

The muon is one of leptons which has no interaction with nuclei. Virtual process and bremsstrahlung from muon are considered for a significant source of nuclear reaction. A few reports on the nuclear reaction with fast muon have been reported [2, 3]. We had measured radioisotopes produced in muon irradiation environment to research penetration and nuclear reaction on the muon, focusing on long life nuclide. Physical property on penetration has been compared with reported values determined at muon beam line.

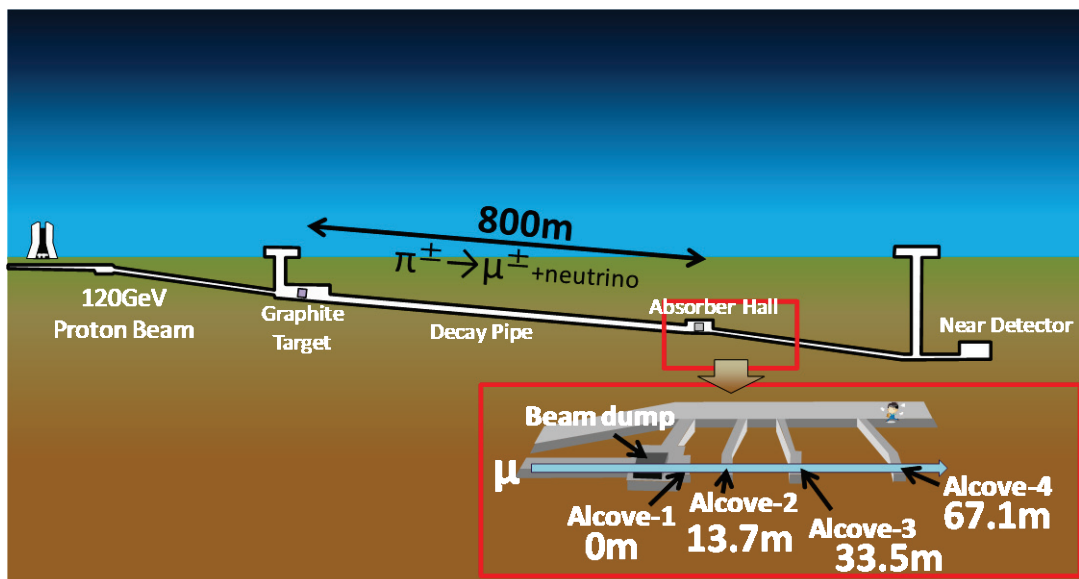


Fig. 1. Schematic diagram of NuMI beam line of Fermi National Accelerator Laboratory.

Muon irradiation was performed at the NuMI beam line of Fermi National Accelerator Laboratory. 120 GeV of primary protons were bombarded with a graphite target to produce pions. The pions were focused with 2 magnetic horns and decayed to muons and neutrinos in a decay pipe with length

¹ High Energy Research Organization

² Japan Atomic Energy Agency

³ Kyoto University Research Reactor Institute

⁴ Fermi National Accelerator Laboratory

of 675 m. Then, the muons were passed through an iron beam dump and rock. Fig. 1 shows the beam line of NuMI. There are 4 rooms at depths of 0 m, 13.7 m, 33.5 m, and 67.1 m from rock surface. The rooms are named Alcove-1, Alcove-2, Alcove-3, and Alcove-4, respectively. The samples of sodium chloride and calcium carbonate were installed in each room for the irradiation. The irradiation was carried out for 3 month.

Chlorine-36 in the irradiated samples were analyzed by an Accelerator Mass Spectrometry (AMS) at University of Tsukuba. The samples of sodium chloride and calcium carbonate were dissolved in water and nitric acid, respectively. Carrier of natural chloride ion was added to the calcium carbonate sample. The chloride ion was precipitated as silver chloride. Subsequently, reduction of sulfur ion was carried out using barium nitrate solution. The purified samples were subjected to the AMS measurement.

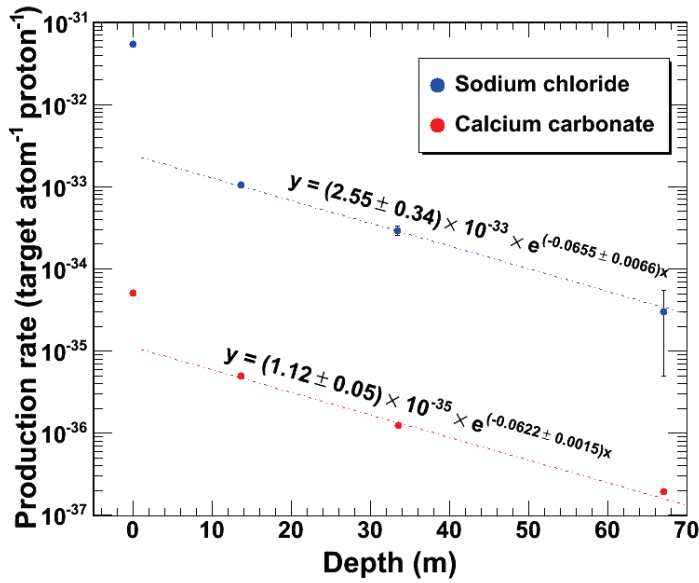


Fig. 2. Depth profile of production rates.

The production rates at Alcove-1 (0 m) are observed to be higher than the trend expected from Alcove-2, 3 and 4. Each data except for Alcove-1 could be fitted using an exponential function with slopes (m^{-1}) of $(-6.55 \pm 0.66) \times 10^{-2}$ for sodium chloride and $(-6.22 \pm 0.15) \times 10^{-2}$ for calcium carbonate.

Attenuation length (g/cm^2) could be calculated from a rock density and the slope. The attenuation lengths were calculated to be $4100 (g/cm^2)$ for sodium chloride and $4300 (g/cm^2)$ for calcium carbonate using $2.65 (g/cm^3)$ for the rock density. The lengths of present work correspond well with reported values of 5300 by Braucher et al. [2] and 4360 by Heisinger et al [3]. Information on muon flux and energy spectrum using Monte Carlo code of Geant4 and MARS etc. are required for more detailed discussion as a future plan.

References

- [1] H.K.M. Tanaka, T. Nakano, S. Takahashi, J. Yoshida and K. Niwa, Nucl. Instru. Meth. A575(2007)489.
- [2] R. Braucher, E.T. Brown, D.L. Bourlès and F. Colin, Earth Planet. Sci. Lett. 211(2003)251.
- [3] B. Heisinger, D. Lal, A.J.T. Jull, P. Kubik, S. Ivy-Ochs, S. Neumaier, K. Knie, V. Lazarev and E. Nolte, Earth Planet. Sci. Lett. 200(2002)345.

4.5 Production rates of ^{36}Cl for target elements in chondritic meteorites (II)

Y. Hamanaka¹, Y. Oura¹, M. Ebihara¹, K. Sasa, Y. Nagashima, T. Takahashi, Y. Tosaki, Y. Matsushi², M. Matsumura, T. Amano, K. Sueki, N. Kinoshita, K. Bessho³, H. Matsumura³.

^{36}Cl is one of the cosmogenic radionuclides found in meteorites and produced by several nuclear reactions such as proton and neutron induced spallation reactions and neutron capture reaction. Cross sections of those reactions depend on particle energies characteristically. Thus it is suggested that additional information must be obtained from ^{36}Cl production rates normalized by a weight of target element (in dpm/kg) for individual target element. So, we have been trying to determine production rates of ^{36}Cl , especially one from $^{35}\text{Cl}(n, \gamma)$ reaction [1, 2]. Last year ^{36}Cl contents and chemical compositions were determined in several different mineral phases separated from two chondritic meteorites fragments, Gold Basin and Gao[2]. This year Cl concentrations in separated phases were determined by radiochemical photon activation analysis (RPAA) and production rates of ^{36}Cl were calculated. And ^{36}Cl contents were determined in additional Gold Basin fragments.

Chemical composition of several silicate phases separated from two fragments of Gold Basin and one fragment of Gao were already determined by instrumental neutron activation analysis (INAA) last year. Their Cl concentrations were determined by radiochemical photon activation analysis (RPAA). And ^{36}Cl contents in new fragments of Gold Basin were determined by same manner in [2]. Chemical compositions of new fragment were not still determined.

Production rates were calculated from combination of Cl concentration by RPAA, the other target elemental concentration by INAA and ^{36}Cl contents in several phases. Since the number of phases with different chemical compositions was insufficient to calculate production rates for whole target elements (Co, Ni, Fe, Mn, Cr, V, Ti Sc, Ca, and K), production rates for several target element groups, (Ca+K), (Fe+Ni) and Cl, were calculated. In this case contribution of ^{36}Cl production from the other target elements was ruled out because of their trace elemental concentration.

Production rates of ^{36}Cl calculated by least square method (LSQM) and alternative least square method (ALSQM) are listed in Table 1. Chlorine concentration in both metal phase and acid - dissolved phase were not determined by RPAA. For LSQM,

Cl concentration in metal phase was assumed to be 0 and one in acid - dissolved phase was estimated from ones in silicate phase and acid-insoluble phase. ALSQM can calculate production rates under that Cl concentration values in these two phases were defective values. Production rate of ^{36}Cl for the

Table 1 Production rates (dpm/kg) of ^{36}Cl in Gold Basin.

	Target	LSQM	ALSQM
Fragment 1	Cl	41000	33000
	K + Ca	16	89
	Fe + Ni	2.5	2.5
Fragment 2	Cl	44000	30000
	K + Ca	8.0	56
	Fe + Ni	1.6	1.6

¹ Graduate School of Science and Engineering, Tokyo Metropolitan University

² MALT, University of Tokyo

³ Radiation Science Center, High Energy Accelerator Research Organization

reaction induced by neutrons ($^{35}\text{Cl}(n, \gamma)$ and $^{37}\text{Cl}(n, 2n)$) were obtained only experimentally for the first time. Since $^{35}\text{Cl}(n, \gamma)$ reaction cross section of thermal neutron is very higher than spallation reaction by proton, production rate for Cl is extremely larger than ones for (K + Ca) and (Fe + Ni). Difference between calculated production rates for (K + Ca) elements by LSQM and ALSQM was significant. This difference is supposed to be caused that Ca and K concentrations in phases obtained in this work were smaller compared to Fe and Ni concentrations. We have to prepare a phase that K and Ca are major composition to obtain more accurate production rate for (K + Ca).

Welten et al.[3] determined ^{36}Cl and ^{10}Be contents in 15 fragments of Gold Basin and estimated contribution of spallation reaction and neutron capture reaction for ^{36}Cl production in conjunction with a model calculation. In Fig.1, their estimation and our result for silicate phases are compared. Our values are consistent with estimation by Welten et al., thus production rates obtained in this work are concluded to be reasonable values.

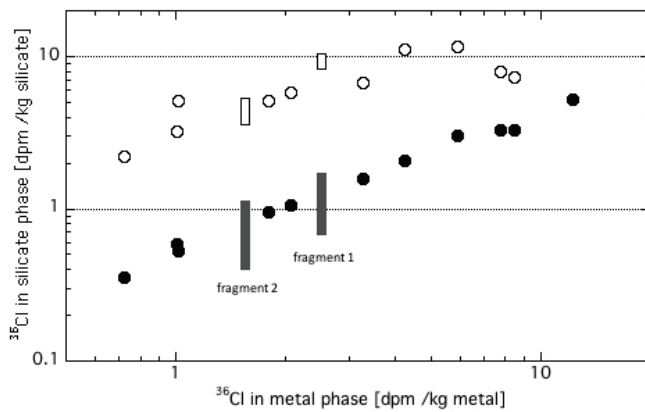


Fig.1 Contents of ^{36}Cl in silicate phase by spallation reaction (closed symbols) and neutron capture reaction (open symbols). Squares show results in this work and circles by Welten et al. [3]. Length of square involves an uncertainty.

^{36}Cl contents in metal phases of new fragments of Gold Basin were different from ones in fragments 1 and 2. This suggests that 4 fragments were originated with different depths in the meteoroid. Using new fragments, additional production rates will be calculated and depth profile of production rate will be evident.

References

- [1] Y. Oura, S. Yamazaki, M. Ebihara, Y. Tosaki, K. Sasa, Y. Nagashima, T. Takahashi, Y. Tosaki, Y. Matsushi, M. Tamari, K. Sueki, H. Matsumura, K. Bessho, and T. Miura, *UTTAC Annual Report 2006* (2007) 39.
- [2] Y. Hamanaka, Y. Oura, M. Ebihara, K. Sasa, Y. Nagashima, T. Takahashi, Y. Tosaki, Y. Matsushi, M. Tamari, T. Amano, K. Sueki, K. Bessho, N. Kinoshita, *UTTAC Annual Report 2008* (2009) 27.
- [3] K. C. Welten, M. W. Caffee, I. Leya, J. Masarik, K. Nishiizumi, and R. Wieler, *Meteorit. Planet. Sci.* **38** (2003) 157.

5.

INTERDISCIPLINARY RESEARCH

5.1 Trace-element analysis of fluid inclusions in the Tsushima granite, Japan

M. Kurosawa, S. Ishii and K. Sasa

Introduction

Fluid released from granitic magma during solidification plays a key role in formation of various metal-ore deposits, hydrothermal alteration, and chemistries of deep groundwater around granite bodies. A part of the fluid is normally trapped as fluid inclusions in the solidified granite and surrounding rocks. Thus, the fluid inclusions provide useful information about chemistries and behaviors of the fluid. The Miocene granite pluton in Tsushima Islands accompanies the largest Pb-Zn metal-ore deposits in southwestern Japan and is well known for its abundant hypersaline fluid-inclusions in quartz crystals [1]. Chemical analyses of the fluid inclusions, therefore, are expected as an information source about genesis of the granite-derived fluids and its large-scale metal transport in the island arc. For these reasons, we analyzed trace metal-elements in the fluid inclusions at the Tsushima granite by using micro-PIXE.

Sample

The Tsushima granite, Nagasaki prefecture, Japan, is mainly composed of biotite granites and contains abundant miarolitic cavities and rarely quartz veins. The estimated emplacement level is 2-6 km deep [2]. Quartz in the granite and the miarolitic cavities includes so many polyphase fluid inclusions with large daughter crystals of halite, calcite, and hematite (Fig. 1). In this study, we focused fluid inclusions in the miarolitic cavities to investigate an original composition of fluids released during solidification of the granite. Salinities of polyphase inclusions in the cavities were of 28-48 wt % NaCl eq. and the homogenizing temperatures (T_h) ranged from 480 to 200 °C. Vapor- and liquid-rich two-phase inclusions were also included. Two-phase inclusions of the cavities showed almost T_h of 400-200 °C. Measured inclusions were an ellipsoidal or negative-crystal shape, and the inclusion depths were less than 10 μm .

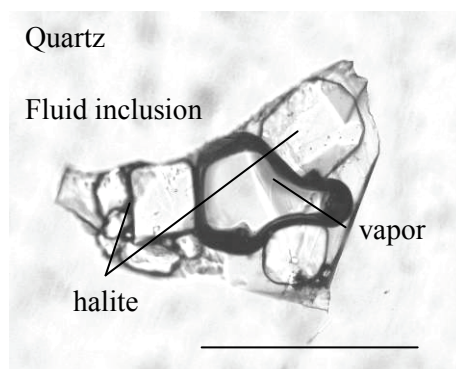


Fig.1. Photomicrograph of polyphase fluid inclusion in quartz crystal from a miarolitic cavity at the Tsushima granite, Japan. A large bubble and many daughter crystals of halite, calcite and so on are present in the inclusions. Scale bar is a 100 μm .

Experimental

The PIXE analyses were performed at the 1MV Tandatron. A 1.0 to 5.0 nA beam of 1.92-MeV proton was focused to a 100 x 100 μm spot on the sample. The beam incidence was normal to the sample surface, and the X-ray measurement take-off angle was 45° (Fig. 2). The characteristic X-rays excited by the incident beam were collected by the Si(Li) X-ray-energy detector with a nominal resolution of 153 eV at 5.9 keV. A 55- μm -thick Mylar film was used to attenuate the intense X-rays from the predominant light elements.

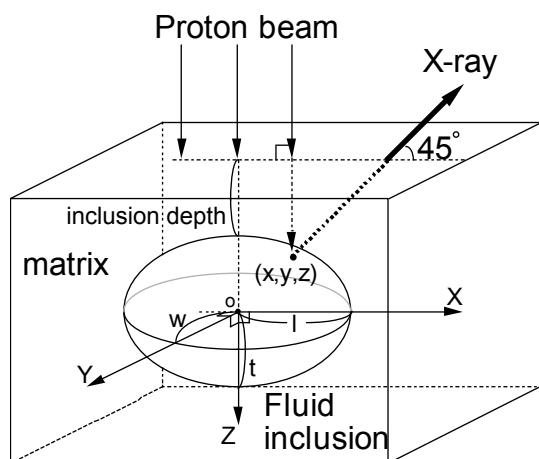


Fig.2. Schematic geometry for PIXE analysis of fluid inclusion.

Results and Discussion

PIXE spectrum of a polyphase inclusion in the cavities is shown in Fig. 3. Most of the inclusions demonstrated the similar X-ray spectra. Element concentrations of the polyphase inclusions were as follows: ~25 wt.% for Cl, 7 wt.% for Fe, 1-5 wt.% for K, Ca and Mn, 7000 ppm for Ba, 1000-3000 ppm for Zn, Pb, Cu, and Br, 100-300 ppm for Rb and Sr. The compositions are thought to correspond to the original contents of hydrothermal fluid released from the Tsushima granite during solidification. The determined values are several times higher than the values of polyphase inclusions in miarolitic quartz from the Miocene Kofu granite, Japan, that has emplacement level, 5-8 km deep [5]. The Tsushima granite solidified at extensively shallower level (2-6 km deep), so that a hypersaline fluid were easily formed by decompression boiling during generation of the hydrothermal fluids. The high contents of transition-metal elements in the polyphase inclusions were also attributable to the element partitioning at the boiling. Thus, a shallow emplacement level of granite body is important to formation of granite-derived fluids with high salinity and high metal content.

References

- [1] H. Imai et al., Mining Geol. Spec. Issue, 3 (1971) 321.
- [2] K. Shin et al., Res. Geol, 59 (2009), 25.
- [3] M. Kurosawa et al., Geochim. Cosmochim. Acta, 67 (2003), 4337.
- [4] M. Kurosawa et al., Nucl. Instr. and Meth. B266 (2008), 3633.
- [5] M. Kurosawa et al., Island Arc, 19 (2010), 40.

The total charge was determined by integrating the target currents, and all samples were analyzed to the integrated charges of 0.5 to 5.0 μC . Analytical points were chosen based on optical viewing using a CCD camera mounted on the microscope [4]. Quantification was performed based on the model of Kurosawa et al. [3, 4]. By using the model, almost trace elements in fluid inclusions at levels of a few ppm to wt.% can be determined with the total analytical error of ± 11 - 40 % [4].

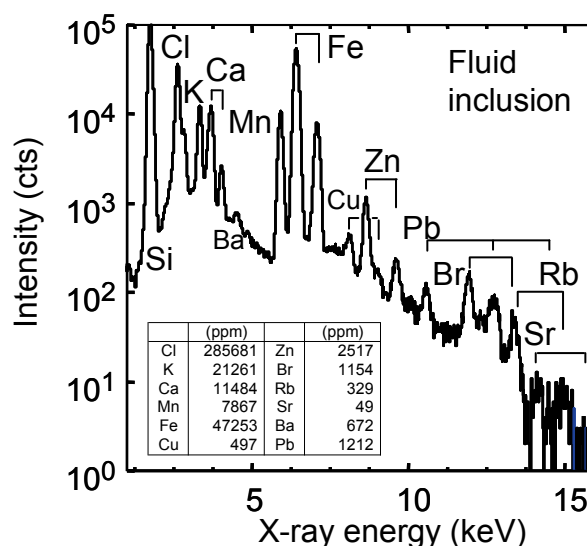


Fig.3. PIXE spectrum of fluid inclusion in quartz crystal from miarolitic cavity at the Tsushima granite, Japan.

5.2 Nanopore fabrication by irradiating accelerated ions for high-sensitivity waveguide-mode sensors

M. Fujimaki¹ and K. Awazu¹

Highly-sensitive molecular detection sensors are required in various fields of application. We have developed an evanescent-field-coupled waveguide-mode (EFC-WM) sensor [1]. Figure 1 is a schematic showing the setup of the sensor. The sensing plate illuminated under the Kretschmann configuration operates as a sensor that is capable of detecting modifications in the dielectric environment near the waveguide surface with superior sensitivity by measuring change in reflectivity [1]. Sensitivity of an EFC-WM sensor strongly depends on the optical constants of its reflecting layer. By theoretical calculation and experiments, we found that Si is an ideal material for the reflecting layer [2]. Based on this finding, we developed a monolithic sensing plate consisting of a SiO₂ glass substrate and a thin single crystalline Si layer, the surface of which is thermally oxidized to form a SiO₂ glass waveguide [3].

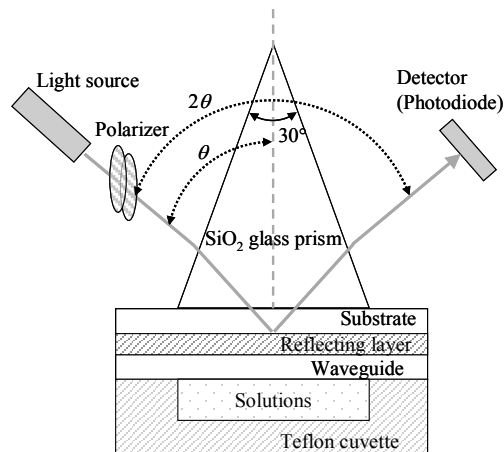


Fig.1. Schematic of the setup of the EFC-WM sensor using the Kretschmann configuration.

We have reported that a significant enhancement of sensitivity of EFC-WM sensors was achieved by perforating the waveguide, in which selective etching of latent tracks formed in the waveguide by swift heavy ion irradiation was used. The monolithic sensing plate is suitable for the nano perforation process [3]. In the present research, we examined the correlation between the sensitivity of the sensor and the sizes and densities of nano holes formed in the waveguide of the monolithic sensing plate. The waveguide was perforated by sequential swift-heavy-ion irradiation and etching with hydrofluoric acid (HF) vapor. Ion irradiation was performed by using the 12 UD Pelletron tandem accelerator at the University of Tsukuba, and the waveguide was irradiated with Au ions at room temperature in a vacuum of about 5×10^{-4} Pa. The average acceleration energy was 137 MeV. For the vapor etching, the irradiated plate and a 20% aqueous solution of HF were placed in a container so that the plate was not immersed in the solution but was suspended close to its surface. The resulting nano holes were observed by scanning electron microscopy (SEM; Hitachi High-Technologies, S4800).

Figures 2(a), 2(b), and 2(c) show SEM images of waveguides, in which nano holes were fabricated. The densities of the nano holes formed in the waveguides in Figs. 2(a), 2(b), and 2(c) are 5×10^9 , 8×10^9 , and $8 \times 10^9 \text{ cm}^{-2}$, respectively. The average diameters of the holes in Figs. 2(a), 2(b), and 2(c) are 30, 30, and 60 nm, respectively. Figures 3(a), 3(b), and 3(c) show reflectance properties of the sensors using the monolithic sensing plates with the perforated waveguides shown in Figs. 2(a), 2(b), and 2(c), respectively. The red circles and the black circles show the reflectance with and without protein adsorption on the waveguide surfaces, respectively. The values of shifts in the peak positions correspond to the sensitivities of the sensors. According to the result, larger number and larger diameter of the holes result in a better sensitivity. The developed sensor is highly sensitive. We are expecting that the sensor can be applied for medical technology, pharmacy, and environmental science.

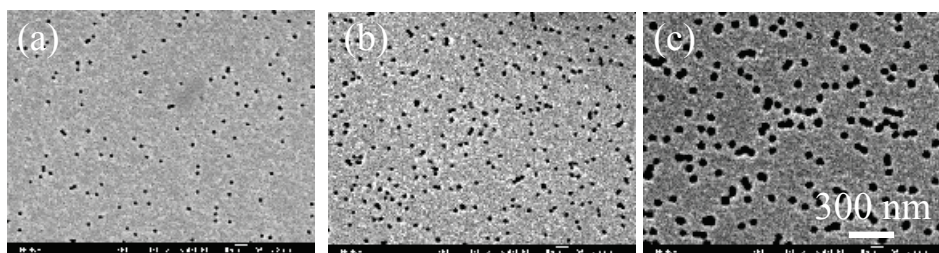


Fig. 2. SEM images of waveguides, in which nano holes were fabricated. The densities of the nano holes in (a), (b), and (c) are 5×10^9 , 8×10^9 , and $8 \times 10^9 \text{ cm}^{-2}$, respectively. The average diameters of the holes in (a), (b), and (c) are 30, 30, and 60 nm, respectively.

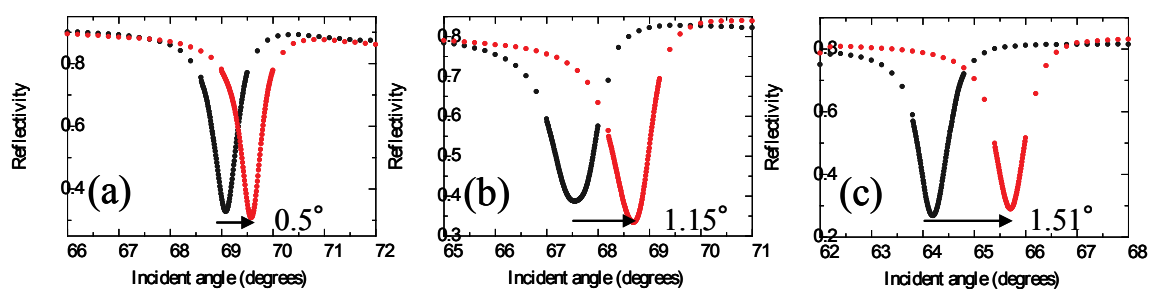


Fig.3. Reflectance properties of the sensors using the monolithic sensing plates with the perforated waveguides shown in Figs. 2(a), 2(b), and 2(c). The red circles and the black circles show the reflectance with and without protein adsorption on the waveguide surfaces, respectively.

This study was supported by Industrial Technology Research Grant Program in 2009 from New Energy and Industrial Technology Development Organization (NEDO) in Japan.

References

- [1] M. Fujimaki et al., *Microelectron. Eng.* **84** (2007) 1685.
- [2] M. Fujimaki et al., *Nanotechnology* **19** (2008) 095503.
- [3] M. Fujimaki et al., *Opt. Express* **16** (2008) 6408.

¹ National Institute of Advanced Industrial Science and Technology (AIST)

6. LIST OF PUBLICATIONS

The publications listed here are those released in the fiscal year 2009 by all the workers listed on p.58.

6.1 Journals

ACCELERATOR AND EXPERIMENTAL FACILITIES

1. K. Sasa, Meeting report: Report on the 11th International Conference on Heavy Ion Accelerator Technology (HIAT09), Journal of the Particle Accelerator Society of Japan, Vol. 6(3) (2009) 251-255.
2. Kimikazu Sasa, Tsutomu Takahashi, Yuki Tosaki, Yuki Matsushi, Keisuke Sueki, Michiko Tamari, Takahiro Amano, Toshiyuki Oki, Shozo Mihara, Yoshihiro Yamato, Yasuo Nagashima, Kotaro Bessho, Norikazu Kinoshita, Hiroshi Matsumura, Status and research programs of the multinuclide accelerator mass spectrometry system at the University of Tsukuba, Nuclear Instruments and Methods in Physics Research B 268 (2010) 871-875.

NUCLEAR PHYSICS

2. Daiya Kaji, Kouji Morimoto, Nozomi Sato, Takatoshi Ichikawa, Eiji Ideguchi, Kazutaka Ozeki, Hiromitsu Haba, Hiroyuki Koura, Yuki Kudou, Akira Ozawa, Takayuki Sumita, Takayuki Yamaguchi, Akira Yoneda, Atsushi Yoshida, Kosuke Morita, Production and Decay Properties of ^{263}Hs , J. Phys. Soc. Jpn., Vol.78, No.3, (2009) p.035003.
3. K.Tanaka, T.Yamaguchi, T.Suzuki, T.Ohtsubo, M.Fukuda, D.Nishimura, M.Takechi, K.Ogata, A.Ozawa, T.Izumikawa, T.Aiba, N.Aoi, H.Baba, Y.Hashizume, K.Inafuku, N.Iwasa, K.Kobayashi, M.Komuro, Y.Kondo, T.Kubo, M.Kurokawa, T.Matsuyama, S.Michimasa, T.Motobayashi, T.Nakabayashi, S.Nakajima, T.Nakamura, H.Sakurai, R.Shinoda, M.Shinohara, H.Suzuki, E.Takeshita, S.Takeuchi, Y.Togano, K.Yamada, T.Yasuno, M.Yoshitake, Observation of a Large Reaction Cross Section in the Drip-Line Nucleus ^{22}C , Phys. Rev. Lett. 104, 062701 (2010).
4. N.Aoi, E.Takeshita, H.Suzuki, S.Takeuchi, S.Ota, H.Baba, S.Bishop, T.Fukui, Y.Hashimoto, H.J.Ong, E.Ideguchi, K.Ieki, N.Imai, M.Ishihara, H.Iwasaki, S.Kanno, Y.Kondo, T.Kubo, K.Kurita, K.Kusaka, T.Minemura, T.Motobayashi, T.Nakabayashi, T.Nakamura, T.Nakao, M.Niikura, T.Okumura, T.K.Ohnishi, H.Sakurai, S.Shimoura, R.Sugo, D.Suzuki, M.K.Suzuki, M.Tamaki, K.Tanaka, Y.Togano, K.Yamada, Development of Large Deformation in ^{62}Cr , Phys.Rev.Lett. 102, 012502-012505 (2009).
5. Y.Ichikawa, T.K.Onishi, D.Suzuki, H.Iwasaki, T.Kubo, V.Naik, A.Chakrabarti, N.Aoi, B.A.Brown, N.Fukuda, S.Kubono, T.Motobayashi, T.Nakabayashi, T.Nakamura, T.Nakao, T.Okumura, H.J.Ong, H.Suzuki, M.K.Suzuki, T.Teranishi, K.N.Yamada, H.Yamaguchi, H.Sakurai, β decay of the proton-rich nucleus ^{24}Si and its mirror asymmetry, Phys. Rev. C 80, 044302-044313 (2009).

6. S.Takeuchi, N.Aoi, T.Motobayashi, S.Ota, E.Takeshita, H.Suzuki, H.Baba, T.Fukui, Y.Hashimoto, K.Ieki, N.Imai, H.Iwasaki, S.Kanno, Y.Kondo, T.Kubo, K.Kurita, T.Minemura, T.Nakabayashi, T.Nakamura, T.Okumura, T.K.Onishi, H.Sakurai, S.Shimoura, R.Sugou, D.Suzuki, M.K.Suzuki, M.Takashina, M.Tamaki, K.Tanaka, Y.Togano, K.Yamada, Low-lying states in ^{32}Mg studied by proton inelastic scattering, *Phys.Rev. C* 79, 054319-054329 (2009).
7. S.Takeuchi, N.Aoi, H.Baba, T.Kubo, T.Motobayashi, K.Tanaka, K.Yamada, T.Fukui, S.Ota, Y.Hashimoto, Y.Kondo, T.Nakabayashi, T.Nakamura, T.Okumura, K.Ieki, S.Kanno, K.Kurita, R.Sugou, E.Takeshita, Y.Togano, N.Imai, T.Minemura, H.Iwasaki, T.K.Onishi, H.Sakurai, D.Suzuki, H.Suzuki, M.K.Suzuki, S.Shimoura, M.Tamaki, Study of low-lying states in ^{32}Mg , *Int. J. Mod. Phys. E* 18, 2025-2029 (2009).

MATERIALS AND CLUSTER SCIENCE

8. U. Kadhane, J.U. Andersen, E. Bonderup, B. Concina, P. Hvelplund, M.-B. Suhr Kirketerp, B. Liu B, S.Brøndsted Nielsen, S. Panja, J. Rangama, K. Støchkel, S. Tomita, H. Zettergren, K. Hansen, A. E. K. Sundén, S. E. Canton, O. Echt, J. S. Forster, "Near-infrared photoabsorption by C_{60} dianions in a storage ring", *J. Chem. Phys.* 131, (2009) 014301 (1-7)
9. Hideyuki Arai, Hiroshi Kudo, Shigeo Tomita, and Satoshi Ishii, "Suppression Mechanism of Electron Emission under Fast Cluster Impact on Solids", *J. Phys. Soc. Jpn.* 78, (2009) 104301 (1-5)
10. Shaoqiang Chen, Akira Uedono, Shoji Ishibashi, Shigeo Tomita, Hiroshi Kudo, and Katsuhiro Akimoto, "Effect of V/III flux ratio on luminescence properties and defect formation of Er-doped GaN", *Appl. Phys. Lett.* 96, (2010) 051907 (1-3)
11. H. Kudo, H. Arai, S. Tomita, S. Ishii, T. Kaneko, "Electron emission from surfaces bombarded by MeV atom clusters", *Vacuum* 84, (2010) 1014-1017
12. Yoshiaki Hata, Yasushi Kanke, Kenji Ohoyama, and Eiji Kita, Site Preference of Fe Ion in $\text{SrV}_{6-x}\text{Fe}_x\text{O}_{11}$, *J. Phys. Soc. Jpn.* 78 No.5 (2009) 054703 (4 pages)
13. S. Luo, S. Kohiki, K. Okada, A. Kohno, T. Tajiri, M. Arai, S. Ishii, D. Sekiba, M. Mitome, F. Shoji, "Effects of hydrogen in working gas on valence states of oxygen in sputter-deposited indium thin oxide thin films", *Applied Materials and Interfaces*, 2 (2010) 663-668.
14. J. Oh, T. Kondo, D. Hatake, Y. Iwasaki, Y. Honma, Y. Suda, D. Sekiba, H. Kudo, J. Nakamura, "Significant reduction in adsorption energy of CO on platinum clusters on graphite", *The Journal of Physical Chemistry Letters*, 1 (2010) 463-466.
15. D. Sekiba, M. Horikoshi, S. Abe, S. Ishii, "Mg segregation in Mg-rich Mg-Ni switchable mirror studied by Rutherford backscattering, elastic recoil detection analysis, and nuclear reaction analysis", *Journal of Applied Physics*, 106 (2009) 114912-1-5.

16. Takahiro Kondo, Yosuke Iwasaki, Yujiro Honma, Yoshiteru Takagi, Susumu Okada and Junji Nakamura, Formation of nonbonding π electronic states of graphite due to Pt-C hybridization, *Phys. Rev. B*, 80, 233408- 1~4, (2009).
17. Takahiro Kondo, Masataka Sakurai, Tatsuo Matsushima, and Junji Nakamura F Angle resolved intensity and velocity distributions of N_2 desorbed by N_2O decomposition on Rh(110), *Journal of Chemical Physics*, Vol. 132, 134714- 1~9 (2009).

ACCELERATOR MASS SPECTROMETRY

18. Norikazu Kinoshita, Hiroshi Matsumura, Kotaro Bessho, Akihiro Toyoda, Kazuyoshi Masumoto, Yuki Matsushi, Kimikazu Sasa, Tsutomu Takahashi, Shozo Mihara, Toshiyuki Oki, Masumi Matsumura, Yuki Tosaki, Keisuke Sueki, Michiko Tamari, Yasuo Nagashima, Depth Profile of Radioactivity Induced in the Thick Concrete Shield in EP1 Beam Line at the KEK 12-GeV Proton Synchrotron Facility, *Nuclear Technology*, Volume 168, Number 3, 2009, Pages 694-699.
19. Kimikazu Sasa, Yuki Matsushi, Yuki Tosaki, Michiko Tamari, Tsutomu Takahashi, Yasuo Nagashima, Kazuho Horiuchi, Hiroyuki Matsuzaki, Yasuyuki Shibata, Motohiro Hirabayashi, Hideaki Motoyama, Measurement of cosmogenic ^{36}Cl in the Dome Fuji ice core, Antarctica: Preliminary results for the Last Glacial Maximum and early Holocene, *Nuclear Instruments and Methods in Physics Research B* 268 (2010) 1193-1196.
20. Yuki Tosaki, Gudrun Massmann, Norio Tase, Kimikazu Sasa, Tsutomu Takahashi, Yuki Matsushi, Michiko Tamari, Yasuo Nagashima, Kotaro Bessho, Hiroshi Matsumura, Distribution of $^{36}Cl/Cl$ in a river-recharged aquifer: Implications for the fallout rate of bomb-produced ^{36}Cl . *Nuclear Instruments and Methods in Physics Research B* 268 (2010) 1261-1264.
21. Yuki Matsushi, Kimikazu Sasa, Tsutomu Takahashi, Keisuke Sueki, Yasuo Nagashima, Yuki-nori Matsukura, Denudation rates of carbonate pinnacles in Japanese karst areas: Estimates from cosmogenic ^{36}Cl in calcite, *Nuclear Instruments and Methods in Physics Research B* 268 (2010) 1205-1208.

INTERDISCIPLINARY RESEARCH

23. K. Nomura, Y. Ohki, M. Fujimaki, X. Wang, K. Awazu, T. Komatsubara, Plasmonic activity on gold nanoparticles embedded in nanopores formed in a surface layer of silica glass by swift-heavy-ion irradiation, *NANOTECHNOLOGY*, 20-47, pp.475306-1-475306-7, 2009/10
24. Makoto Fujimaki, Koichi Awazu, Development of high-sensitivity molecular adsorption detection sensors, *Synthesiology*, 2-2, pp.147-158, 2009/06
25. Subash C.B. Gopinath, Koichi Awazu, Makoto Fujimaki, Junji Tominaga, Kailash C. Gupta, Penmetcha K. R. Kumar, Monitoring biological interactions using perforated evanescent-field-coupled waveguide-mode nanobiosensors, *Nucleic Acids symposium series*, 53-, pp.93-94A2009/09
26. Masanori Kurosawa, Satoshi Ishii, Kimikazu Sasa, Trace-element compositions of single fluid inclusions in the Kofu granite, Japan: Implications for compositions of granite-derived fluids, *The Island Arc*, Volume 19, Number 1, March 2010, 40-59.
27. A. Tominaga, T. Kato, T. Kubo, and M. Kurosawa, Preliminary analysis on the mobility of trace incompatible elements during the basalt and peridotite reaction under uppermost mantle conditions, *Physics of the Earth and Planetary Interiors*, 174, 50-59, (2009).
28. Y. Ogawa, R. Mori, N. Hirano, A. Takahashi, M.M. Mohiuddin, H. Sato, T. Tsunogae, M. Kurosawa, H. Taniguchi, and T. Chiba, Knocker catalogue of the Mineoka ophiolite belt, Boso Peninsula, Japan, *Earth Evolution Sciences*, 3, 3-25, (2009).

6.2 International conferences

1. Kimikazu Sasa (Invited talk), Multi-nuclide AMS system at the University of Tsukuba, 7th Japan-China Joint Nuclear Physics Symposium, November 9 - 13, 2009, University of Tsukuba, Ibaraki, Japan
2. Kimikazu Sasa, Tsutomu Takahashi, Yasuo Nagashima, Yuki Tosaki, Keisuke Sueki, Toshiyuki Oki, Takahiro Amano, Hiroshi Matsumura, Kotaro Bessho, Norikazu Kinoshita, Yuki Matsushi, Progress of an accelerator mass spectrometry system at the Tsukuba 12UD Pelletron tandem accelerator, The 11th edition of the International Conference "Heavy Ion Accelerator Technology - HIAT", Venice, Italy, from 8 to 12 June 2009.
3. K. Sasa, T. Takahashi, Y. Nagashima, Y. Tosaki, K. Sueki, Y. Takaya, N. Kinoshita, T. Amano, J. Kitagawa, K. Kurozumi, M. Matsumura, H. Matsumura, K. Bessho, Y. Matsushi, Application of Cl-36 AMS to geo-environmental sciences at the University of Tsukuba, 3rd East Asian Symposium on Accelerator Mass Spectrometry (EA-AMS-3), 19th-22nd October, 2009, Xi'an AMS Center, Xi'an China.
4. Kimikazu Sasa, Yuki Matsushi, Yuki Tosaki, Michiko Tamari, Tsutomu Takahashi, Yasuo Nagashima, Hiroyuki Matsuzaki, Kazuho Horiuchi, Yasuyuki Shibata, Motohiro Hirabayashi and Hideaki Motoyama, Cosmogenic ^{36}Cl record in an ice core at the Dome Fuji station, Antarctica from the Last Glacial Maximum to Holocene, The 2nd International Symposium on the Dome Fuji ice core and related topics, November 18-20, 2009. NIPR in Tachikawa City, Tokyo.
5. Yuki Matsushi, Kimikazu Sasa, Tsutomu Takahashi, Keisuke Sueki, Yasuo Nagashima, Yuki-nori Matsukura, Denudation rate of karst surfaces in Japan: estimates from cosmogenic ^{36}Cl , 7th INTERNATIONAL CONFERENCE ON GEOMORPHOLOGY, Ancient Landscapes Modern Perspectives, Melbourne, Australia, July 6-11, 2009.
6. S. Merchel, W. Bremser, V. Alfimov, M. Arnold, G. Aumaître, L. Benedetti, D. L. Bourlés, R. Braucher, M. Caffee, M. Christl, L. K. Fifield, R. C. Finkel, S. P. H. T. Freeman, A. Ruiz-Gómez, P. W. Kubik, D. H. Rood, K. Sasa, P. Steier, S. G. Tims, A. Wallner, K. M. Wilcken, S. Xu. Be-10 and Cl-36 interlaboratory comparisons: Implications for terrestrial production rates?, CRONUS-EU/CRONUS-Earth Science Workshop, Goldschmidt 2009, June 21 - 26 in Davos, Switzerland.
7. Norikazu Kinoshita, Kazuyoshi Masumoto, Hiroshi Matsumura, Kotaro Bessho, Akihiro Toyoda, Kimikazu Sasa, Yuki Tosaki, Michiko Tamari, Takahiro Amano, Takahashi Tsutomu, Keisuke Sueki, Toshiyuki Oki, Shozo Mihara, Yasuo Nagashima and Yuki Matsushi, Measurement and Monte Carlo simulation of radioactivity produced in concrete shield in EP-1 beam-line at the 12-GeV proton synchrotron facility, KEK, the Fifth International Symposium on Radiation Safety and Detection Technology (ISORD-5), July 15 - 17, 2009, Kitakyushu International Conference Center, Kitakyushu, Japan.

8. H. Kudo, H. Arai, S. Tomita, S. Ishii, and T. Kaneko, Electron emission from surfaces bombarded by MeV atom clusters (Invited talk), 19th International Conference on Ion-Surface Interactions, Zvenigorod, Russia, (2009).
9. Shigeo Tomita, Application of a superconducting detector to experimental studies on molecular fragmentation, Third International Workshop on Electrostatic Storage Devices (invited), Aarhus, June 21 - 25 (2009).
10. Shigeo Tomita, Fullerene fusion induced by highly charged ion impacts on clusters of fullerenes, XXVI International Conference on Photonic, Electronic, and Atomic Collisions, Kalamazoo, USA, 22-28 July (2009).
11. M. Horikoshi, S. Abe, D. Sekiba, Degradation mechanism of Mg₄Ni-H switchable mirror revealed by RBS-ERDA, 19th International Conference on Ion Beam Analysis, University of Cambridge (UK) 7-11 September, (2009).
12. H. Yonemura, D. Sekiba, Y. Kitaoka, T. Narusawa, T. Ito, Y. Iwamura, K. Fukutani, Shallow-depth profiling of hydrogen at gas-surface interfaces, 19th International Conference on Ion Beam Analysis, University of Cambridge (UK) 7-11 September, (2009).
13. D. Sekiba, Y. Kitaoka, H. Yonemura, S. Ogura, T. Narusawa, T. Ito, Y. Iwamura, K. Fukutani, Site-specific 3D hydrogen mapping by micro-beam NRA, 19th International Conference on Ion Beam Analysis, University of Cambridge (UK) 7-11 September, (2009).
14. Takahiro Kondo, Yosuke Iwasaki, Yujiro Honma, Yoshiteru, Takagi, Susumu Okada, Junji Nakamura : Formation of non-bonding electronic states of graphite due to Pt-C hybridization. European conference on surface science 26 (ECOSS26), 30. Aug.- 4. Sep. 2009.
15. June Pyo Oh, Takahiro Kondo, Daigo Hatake, Yujiro Honma, Keitaro Arakawa, Takahiro Machida, Junji Nakamura: Changing of the scattering behavior of He atom beam in different surface state of graphite. European conference on surface science 26 (ECOSS26), 30. Aug.- 4. Sep. 2009.
16. Takahiro Kondo, Yosuke Iwasaki, Yujiro Honma, Yoshiteru, Takagi, Susumu Okada, Junji Nakamura : STM, STS and IETS study of the graphite surface electronically modified by Pt nano-clusters. 10th International Conference on Atomically Controlled Surfaces, Interfaces and Nanostructures, (ACSIN10) 21-25, Sep. 2009.
17. Takahiro Kondo, June Pyo Oh, Daigo Hatake, Yujiro Honma, Keitaro Arakawa, Takahiro Machida, Junji Nakamura : Molecular beam scattering from electronically modified graphite surface by metal nano-clusters and nitrogen ions. 10th International Conference on Atomically Controlled Surfaces, Interfaces and Nanostructures, (ACSIN10) 21-25, Sep. 2009.
18. Evanescent-field-coupled waveguide-mode sensors for molecular adsorption detection, Makoto Fujimaki, Koichi Awazu, Junji Tominaga, FACSS, the Federation of Analytical Chemistry and Spectroscopy Societies, conference 2009CLouisville, KY, USAA2009/10/22.

19. Monitoring biological interactions using perforated evanescent-field-coupled waveguide-mode nanobiosensors, Subash C.B. Gopinath, Koichi Awazu, Makoto Fujimaki, Junji Tominaga, Kailash C. Gupta, Penmetcha K. R. Kumar, The 6th International symposium on Nucleic Acid Chemistry (6ISNAC2009), Gifu, 2009/10/01.

7. THESES

Ph. D. Theses

Hideyuki Arai	Suppression mechanism of electron emission under fast cluster impact on solids
Ken-ichi Nomura (Waseda Univ.)	Fabrication of micro/nano-structured metals and insulators and its applications to devices utilizing optical near-fields
Seung-Jun Yu (Waseda Univ.)	Birefringence induced in silica glass by ion implantation and its applications to waveguide-type optical control devices

M. Sc. Theses

Ken-ichiro Ogawa	Developments of tilted electrode grid ion chamber for measurements of energy loss for RI beams
Yuta Itoh	Developments of cluster ion source for magnetic-field calibration in Rare RI Ring
Tomohiro Ikuyama	Study of reaction between Cu cluster and H ₂ S ions
Masahiro Matsuoka	Mechanism of droplet formation in N ₂ /H ₂ O/SO ₂ under irradiation of 20MeV proton beam
Kensuke Shiba	Extended X-ray-absorption fine structure of Mg ₂ Ni and MgTi hydrides
Masato Horikoshi	Suppression of Mg segregation in Mg-Ni switchable mirror by Si dope
Tatsuya Watanabe	Synthesis of single phase iron nitride thin films with NH ₃ nitridation
Shinji Fujii (Waseda Univ.)	Effects of swift heavy-ion irradiation on the crystal phase control and photocatalytic properties of TiO ₂ substrates

8. SEMINARS

<u>Date</u>	<u>Title and Speaker</u>
2009	
May	20 Systematic study of azimuthal anisotropy for charged hadrons in relativistic nucleus-nucleus collisions at RHIC-PHENIX <i>Maya Shimomura (Univ. of Tsukuba)</i>
Oct	2 He ion microscope and its applications <i>B. Thompson (Carl Zeiss SMT Inc.)</i>
Nov	18 AMS measurements and applications in China Institute of Atomic Energy <i>Jiang Shan (China Institute of Atomic Energy)</i>
Dec	22 Suppression mechanism of electron emission under fast cluster impact on solids <i>Hideyuki Arai (Mitsutoyo Corp.)</i>
2010	
Jan	6 Experimental approach to explosive nucleosynthesis in the universe with RI beams from CRIB <i>S. Kubono (CNS)</i>
Jan	13 Reaction of copper cluster cations Cu_n^+ ($n=1-11$) with H_2S <i>Tomohiro Ikuyama (Univ. of Tsukuba)</i>
	Development of tilted electrode gas ionization chamber for energy-loss measurements of RI beams <i>Ken-ichiro Ogawa (Univ. of Tsukuba)</i>
	Capability of Quark/Gluon-Jet Separation for QGP Study at LHC-ALICE <i>Hiroki Yokoyama (Univ. of Tsukuba)</i>
Jan	20 Multiplicity dependence of the accumulative correlation and mean p_T in $\sqrt{s}=200\text{GeV}$ p+p collisions at RHIC-PHENIX <i>Midori Kajigaya (Univ. of Tsukuba)</i>
	Study of parton-QGP medium interactions by measurements of reaction plane dependence of multi-particle correlations for charged hadrons in $\sqrt{s_{NN}}=200\text{GeV}$ Au+Au collisions at RHIC-PHENIX <i>Eitaro Hamada (Univ. of Tsukuba)</i>

Jan 27 Developments of cluster ion source for magnetic-field calibration in rare RI ring
Yuta Ito (Univ. of Tsukuba)

Jet distribution of two particle correlations for charged hadrons in Cu+Cu collisions at $\sqrt{s_{NN}}=200\text{GeV}$
Mizuki Kimura (Univ. of Tsukuba)

Study of reaction plane and rapidity dependence of inclusive photon - hadron correlation in Au+Au collisions at $\sqrt{s_{NN}} = 200 \text{ GeV}$
Takahito Todoroki (Univ. of Tsukuba)

9. SYMPOSIA

The 7th Japan-China Joint Nuclear Physics Symposium

9-13 November 2009

University Hall, University of Tsukuba

1. Welcome address : *Masafumi Akahira (Vice President, University of Tsukuba)*
2. Welcome address : *Shoji Nagamiya (J-PARC)*
3. In-beam γ -ray spectroscopy of unstable nuclei at RIBF : *Nori Aoi (RIKEN)*
4. Recoiled proton tagged knockout reaction for ^8He : *Yanlin Ye (Peking University)*
5. Pair correlations and pair transfers in neutron-rich nuclei : *Masayuki Matsuo (Niigata University)*
6. Neutron halo in deformed nuclei : *Shangui Zhou (ITP, CAS)*
7. Baryon Interaction from lattice QCD : *Shinya Aoki (University of Tsukuba)*
8. Chiral Symmetry and Axial Anomaly in Quark-Hadron Systems : *Teiji Kunihiro (Kyoto University)*
9. Phase Transitions of Strong Interaction System in Dyson-Schwinger Equation Approach of QCD : *Yuxin Liu (Peking University)*
10. Recent Results from LEPS and Future Prospects at LEPS2 : *Takashi Nakano (RCNP, Osaka University)*
11. Self-consistent covariant description of nuclear spin-isospin resonances : *Jie Meng (Peking University)*
12. Systematic calculation of electric dipole strength with Skyrme-HF plus RPA : *Tsunenori Inakura (University of Tsukuba)*
13. The Study of global dispersive coupled-channel optical potential : *Weili Sun (IAPCM)*
14. Studies of Several Heavy Ion Reactions Around the Coulomb Barriers : *Huanqiao Zhang (CIAE)*
15. Flow Effects on Parton Energy Loss : *Enke Wang (Huazhong Normal University)*
16. ALICE Experiment at LHC : *Toru Sugitate (Hiroshima University)*
17. RIKEN RIBF project : *Hiroyoshi Sakurai (RIKEN)*
18. Status and prospective of HIRFL : *Guoqing Xiao (IMP, CAS)*
19. Research activities at the RCNP cyclotron facility : *Kichiji Hatanaka (RCNP, Osaka University)*
20. Band properties of the transitional nucleus ^{189}Pt : *Wei Hua (IMP, CAS)*
21. Multi-quasiparticle isomers in the vicinity of ^{132}Sn : *Hiroshi Watanabe (RIKEN)*
22. Quantum mechanical effects in tilted axis rotations in ^{182}Os : *Yukio Hashimoto (University of Tsukuba)*
23. Microscopic derivation of five-dimensional collective Hamiltonian of large-amplitude quadrupole motion: application to shape coexistence in proton-rich Se isotopes : *Nobuo Hinohara (RIKEN)*
24. The equation of state of QCD at finite chemical potential and zero temperature : *Hongshi Zong (Nanjing University)*

25. Spin Physics at RHIC : *Yuji Goto (RIKEN)*
26. Pionic pair condensation under finite isospin chemical potential : *Masayuki Matsuzaki (Fukuoka University of Education)*
27. Study of nucleon resonances at EBAC@JLab : *Hiroyuki Kamano (Jefferson Lab)*
28. Studies on the isospin effect and isoscaling behavior in heavy ion collisions : *Deqing Fang (SIAP, CAS)*
29. Experimental proposal to study β -decay properties around $N=126$ nuclei produced by multi-nucleon transfer reactions : *Yutaka Watanabe (KEK)*
30. Recent activities at Tokai tandem accelerator : *Tetsuro Ishii (JAEA)*
31. The progress on RFQ1L and LPT : *Wenxue Huang (IMP, CAS)*
32. The AMS Measurements and Its Application in Nuclear Physics at CIAE : *Shan Jiang (CIAE)*
33. Multi-nuclide AMS system at the University of Tsukuba : *Kimikazu Sasa (University of Tsukuba)*
34. The Nuclear Data Activities Related with ADS in China : *Haihong Xia (CIAE)*
35. Physics with ϕ -Meson Production at STAR : *Xiangzhou Cai (SIAP, CAS)*
36. 3D hydro and hadron cascade model at RHIC and LHC : *Chiho Nonaka (Nagoya University)*
37. The ratio of shear/bulk viscosity over entropy density near phase transition : *Mei Huang (IHEP, CAS)*
38. Experimental studies of quark gluon plasma at RHIC : *Shinichi Esumi (University of Tsukuba)*
39. Shear viscosity of gluon plasma in heavy ion collision : *Qun Wang (University of Science and Technology of China)*
40. Hypernuclear Spectroscopy at KEK : *Hiroyuki Noumi (RCNP)*
41. Recent progress on constraining the asymmetry nuclear EOS at supra-saturation densities in heavy ion collisions : *Zhigang Xiao (Tsinghua University)*
42. Exotic nuclear systems with strangeness: Hypernuclei and Kaonic nuclei : *Akinobu Dote (KEK)*
43. Alpha inelastic scattering and cluster structures in light nuclei : *Takahiro Kawabata (Kyoto University)*
44. α -clustering and Molecular-Orbital States of sd-shell nuclei : *Masaaki Kimura (Hokkaido University)*
45. Decay curve study in a standard electron capture decay : *Takayuki Yamaguchi (Saitama University)*
46. Present status of α -particle condensed states in $4n$ self-conjugate nuclei : *Yasuro Funaki (University of Tsukuba)*
47. Nuclear Astrophysics Studies with the Method of Continuum-Discretized Coupled Channels : *Kazuyuki Ogata (Kyusyu University)*
48. Nucleon superfluidity in asymmetric nuclear matter and neutron star matter : *Wei Zuo (IMP, CAS)*
49. Production ratio of meta-stable isomer in ^{180}Ta by neutrino-induced reactions : *Takehito Hayakawa (JAEA)*
50. Nuclear astrophysics and structure studies using low-energy RI beams at CRIB : *Hidetoshi Yamaguchi (CNS)*
51. New Band Structures in $A=110$ Neutron-Rich Nuclei : *Shengjiang Zhu (Tsinghua University)*
52. Electromagnetic Moment of Proton-Rich ^{28}P and Decomposition of Its Spin : *Kensaku Matsuta (Osaka University)*

53. Gamow-Teller transition of proton-rich nucleus ^{24}Si : *Yuichi Ichikawa (RIKEN)*
54. Three-body force effects in few-nucleon systems : *Souichi Ishikawa (Hosei University)*
55. nd Scattering Observables Derived from the Quark-Model Baryon-Baryon Interaction : *Yoshikazu Fujiwara (Kyoto University)*
56. Calculation of the nd Scattering lengths by a Realistic Nonlocal Gaussian Potential : *Kenji Fukukawa (Kyoto University)*
57. Study of Double Beta Decay of ^{48}Ca with CANDLES : *Saori Umehara (Osaka University)*
58. Preparation and Characterization of Gadolinium Loaded Liquid Scintillator for Daya Bay Neutrino Experiment : *Zhang Zhiyong (IHEP, CAS)*
59. Construction and Beam Commissioning of J-PARC Hadron Experimental Facility : *Yoshinori Sato (KEK)*
60. Nuclear Physics program at HIRFL : *Hushan Xu (IMP, CAS)*
61. Current status and future experimental program of the SHARAQ spectrometer : *Tomohiro Uesaka (CNS, University of Tokyo)*
62. Experimental study of nuclear astrophysics with photon beams : *Tatsushi Shima (RCNP)*
63. In-direct measurements of nuclear astrophysics reactions in CIAE : *Weiping Liu (CIAE)*
64. Spin Resonances in Nuclei, Neutrino-Induced Reactions and Nucleosynthesis in Stars : *Toshio Suzuki (Nihon University)*
65. Measurements of proton-proton momentum correlation functions from the proton-rich nuclei induced reactions : *Yugang Ma (SIAP, CAS)*
66. R-process in Supernovae and Gamma-Ray Bursts : *Toshitaka Kajino (NAO)*
67. Theoretical research on electron scattering with unstable nuclei : *Zhongzhou Ren (Nanjing University)*
68. Shell correction energy and entrance channel effect on the formation of heavy and superheavy nuclei : *Fengshou Zhang (Beijing Normal University)*
69. Superheavy Element Nuclear Chemistry at RIKEN : *Hiromitsu Haba (RIKEN)*
70. Recent results on the studies of high spin states at CIAE : *Lihua Zhu (CIAE)*
71. Quasi-Particle Alignment and Magnetic Rotation of High Spin States Investigated by g-Factor Measurements : *Shengyun Zhu (CIAE)*
72. Nucleon Pair Approximation of the shell model : *Yumin Zhao (Shanghai Jiao Tong University)*
73. Recent progress in shell-model calculations for pfg-shell nuclei : *Michio Honma (Aizu University)*
74. Shell-Model Calculations of $N \approx Z A \approx 50$ Nuclei Employing Realistic NN Interaction : *Furong Xu (Peking University)*
75. Concluding remarks : *Weiping Liu (CIAE)*

**The 22nd Community Meeting on the Electrostatic Particle Accelerators and
their Related Technologies**

16-17, July, 2009

University Hall, University of Tsukuba

1. Opening Address : *H. Kudo (Univ. of Tsukuba)*
2. Status of the tandem accelerator facility at the University of Tsukuba : *K. Sasa, S. Ishii, H. Oshima, H. Kimura, T. Takahashi, Y. Tajima, Y. Yamato, T. Komatsubara, D. Sekiba and H. Kudo (University of Tsukuba)*
3. Status report of MALT, The University of Tokyo : *C. Nakano, H. Matsuzaki, A. Morita, S. Ito, Y. Tsutiya, Y. Miyairi, Y. Matsushi, K. Abe, T. Aze (The University of Tokyo)*
4. Present status of JAEA-Tokai tandem accelerator facility : *M. Matsuda, T. Ishii, Y. Tsukihashi, S. Hanashima, S. Abe, A. Osa, N. Ishizaki, H. Tayama, T. Nakanoya, H. Kabumoto, M. Nakamura, K. Kutsukake, Y. Otokawa and T. Asozu (Japan Atomic Energy Agency)*
5. Progress report of NIRS electrostatic accelerator facility (PASTA & SPICE) : *M. Oikawa, N. Suya, T. Ishikawa, T. Konishi, H. Imaseki (National Institute of Radiological Sciences), H. Iso, Y. Higuchi (Neos Tech Co., Ltd.)*
6. Present Conditions of Tandem Accelerator in Kobe University : *A. Taniike, Y. Furuyama, A. Kitamura (Kobe University)*
7. Progress report of tandem accelerator in NWU : *J. Karimata, N. Fujita, A. Shimada, Y. Inoue, K. ishii and H. Ogawa (Nara Womenfs University)*
8. Status Report of Kyushu University Tandem Accelerator : *T. Morikawa, K. Sagara, T. Noro, T. Wakasa, T. Teranishi, K. Fujita, T. Maeda, and N. Ikeda (Kyushu University)*
9. Current status of the accelerator facility at The Wakasa Wan Energy Research Center : *S. Hatori, T. Kurita, Y. Hayashi, H. Yamada, M. Shimada, M. Hiroto, H. Hamachi, T. Hashimoto, K. Kanai, Y. Nakata, F. Yamaguchi, M. Yodose, T. Odagiri, S. Nagasaki, H. Yamamoto, N. Ohtani, E. Minehara, S. Fukumoto (The Wakasa Wan Energy Research Center)*
10. Present Status and Applications of AMS ^{14}C System at Nagoya University (2009) : *T. Nakamura, M. Minami, T. Oda, A. Ikeda, M. Miyata, T. Ohta, M. Nishida, T. Omori, H. Nishimoto, K. Hayashui, K. Honjyo, K. Matsumoto, Y. Jyomori (Nagoya Univesity), Y. Suya (National Institute for Radiological Sciences) and T. Sekino (Elicon. co. Ltd)*
11. Current status of the compact ^{14}C AMS system at Paleo Labo Co., Ltd. : *S. Itoh, E. Niu, H. Ozaki, M. Hirota, K. Setani, Z. Lomtadze, I. Jorjoliani, K. Kobayashi (Paleo Labo Co., Ltd.)*
12. Present Status of the JAEA-AMS-TONO : *Y. Saito-Kokubu, M. Suzuki, T. Ishimaru (JAEA), A. Nishizawa, Y. Ohwaki, T. Nishio (Pesco Corp., Ltd.)*
13. Equipment improvements of the JAEA-AMS-TONO : *M. Suzuki, Y. Saito-Kokubu, T. Ishimaru (JAEA), A. Nishizawa, Y. Ohwaki, T. Nishio (Pesco Corp., Ltd.)*
14. Upgrade of the Dynamitron Accelerator III : *M. Fujisawa, T. Nagaya, S. Matsuyama, R. Sakamoto, Y. Hashimoto, H. Yamazaki and K. Ishi (Tohoku University)*
15. Development of Proton Beam Writing for Micromachining and Technical Challenges : *H. Nishikawa, Y. Seki, Y. Shiine, T. Kaneko (Shibaura Institute of Technology)*
16. Micro Van de Graaff Generators and their Acceleration Tubes : *E.J. Minehara (The Wakasa Wan Energy Research Center), H. Yano (Wakasa Engineering Co. Ltd.)*
17. Improvement of the AMS Data Integration System : *Y. Yamato, H. Kimura, K. Sasa (University of Tsukuba)*
18. Insulation Breakdown of the Schenkel Column Support : *M. Shimada, S. Hatori, T. Kurita, Y. Hayashi, H. Yamada, H. Hamachi, M. Hiroto, T. Hashimoto, K. Kanai, Y. Nakata, F. Yamaguchi, M. Yodose, S. Nagasaki, T. Odagiri, N. Ohtani, S. Fukumoto, E. Minehara (Wakasa Wan Energy Research Center), N. Ogino, Y. Eto, E. Shimizu (Non-Destructive Inspection Co., Ltd.)*

19. Present Status of the Control System for the JAEA Tokai Tandem : *S. Hanashima (Japan Atomic Energy Agency)*
20. Emission Management of SF₆ gas at the JAEA-Tokai tandem accelerator : *T. Nakanoya, H. Tayama, H. Kabumoto, M. Matsuda, Y. Tsukihashi (Japan Atomic Energy Agency)*
21. Improvement of beam bunching system at KUTL : *K. Fujita, K. Sagara, N. Goto, K. Nakano, R. Iwabuchi, M. Taniguchi, N. Oba, T. Maeda (Kyushu University)*
22. Development of a μ -PIXE System Using Glass Capillary Optics : *J. Hasegawa, H. Fukuda, Y. Oguri (Tokyo Institute of Technology)*
23. Observation of the SEU mapping in the SOI devices induced by microbeam irradiation : *T. Hirao, S. Onoda, T. Makino, T. Ohshima (Japan Atomic Energy Agency), S. Abo, N. Masuda, M. Takai (Osaka University)*
24. Heavy-ion microbeam system for cell irradiation at Kyoto University : *M. Nakamura, S. Makino (Wakayama Medical University), K. Imai, M. Hirose, H. Matsumoto, M. Tosaki, D. Ohsawa, K. Komatsu (Kyoto University), O. Niwa (National Institute of Radiological Sciences), and H. Utsumi (Health Research Foundation)*
25. Luminescence from Sapphire Bombarded by MeV Cluster Ion Beams : *H. Shibata (Kyoto University), Y. Saitoh, A. Chiba, Y. Takahashi, K. Narumi (Japan Atomic Energy Agency)*
26. Nucleation mechanism of water droplets in air under irradiation of 20 MeV protons : *S. Tomita, M. Matsuoka, M. Fujieda, K. Sasa, H. Kudo (University of Tsukuba)*
27. Radiocarbon dating of the silk fabrics laced with colored threads gEzo Nishikih by AMS : *H. Oda, M. Yoshida (Nagoya University), K. Nakamura (Hakodate National College of Technology), H. Amano (Japan Chemical Analysis Center), H. Takimoto (Ohminato High School)*
28. Plan and status to introduce AMS at Yamagata University : *F. Tokanai (Yamagata University)*
29. Open Advanced Facilities Initiative for Innovation (Strategic Use by Industry) at UTTAC : *H. Kudo, Y. Tagishi, H. Naramoto, S. Mihara, T. Oki (University of Tsukuba)*
30. Current Status of Electrostatic Accelerators at TIARA : *A. Chiba, S. Uno, K. Yamada, A. Yokoyama, T. Agematsu, Y. Saitoh, Y. Ishii, T. Satoh, T. Okubo (JAEA), T. Kitano, T. Takayama, T. Orimo, M. Kouka, Y. Aoki, N. Yamada (Beam Operation Service co., Ltd.)*
31. Status of JAEA-AMS-MUTSU in 2008-2009 : *T. Suzuki, S. Otsuka, T. Tanaka, S. Kou, N. Kinoshita, N. Yamamoto (JAEA)*
32. Current Status of High Fluence Irradiation Facility, The University of Tokyo (HIT) : *T. Iwai, T. Omata and M. Uesaka (The University of Tokyo)*
33. Status of the 1 MV Tandetron accelerator at the University of Tsukuba : *S. Ishii, K. Sasa, D. Sekiba, H. Oshima, M. Kurosawa, S. Tomita, and H. Kudo (University of Tsukuba)*
34. Status of dynamitron accelerator : *Y. Hashimoto, M. Fujisawa, T. Nagatani, S. Matsuyama, T. Sakamoto, K. Ishii, H. Yamazaki (Tohoku University)*
35. Development of femto ampere level irradiation system : *S. Ito, A. Morita, H. Matsuzaki (The University of Tokyo)*
36. Influence of the median potential in an electrostatic steerer on beam optics : *T. Asozu, M. Matsuda, K. Kutsukake, M. Nakamura (Japan Atomic Energy Agency)*
37. Operational testing of the microcontroller (PIC) in C language : *M. Nakamura (Japan Atomic Energy Agency)*
38. Recovery of acceleration field gradients of superconducting booster resonators by high pressure water jet rinsing : *H. Kabumoto, S. Takeuchi, N. Ishizaki (Japan Atomic Energy Agency), T. Yoshida, T. Ishiguro, K. Yamaguchi (Atox, co., ltd.)*
39. Development of measurement-and-control devices for JAEA-Tokai tandem accelerator : *K. Kutsukake, M. Makoto, S. Hanashima (Japan Atomic Energy Agency)*

40. Emittance measurement using scintillator luminescence induced by MeV proton beams II : A. Yokoyama, Y. Ishii, A. Chiba, S. Uno, T. Agematsu (Japan Atomic Energy Agency), T. Takayama, M. Koka (Beam Operation. Ltd)
41. Monitoring system of beam transport parameters at Kyushu University Tandem Accelerator : K. Iketani, K. Uechi, M. Shimamoto, T. Fukuda, T. Sato, K. Fujita, H. Minamoto, T. Morikawa, T. Noro, T. Maeda (Kyushu University)
42. Stabilization of AMS System at Kyushu University and Post-bomb ¹⁴C-dating of Botanical Specimen : K. Uechi, K. Iketani, M. Shimamoto, T. Fukuda, T. Morikawa, T. Noro and T. Maeda (Kyushu University)
43. Status report of the Tsukuba AMS system : T. Takahashi, K. Sasa, Y. Nagashima, Y. Tosaki, K. Sueki (University of Tsukuba)
44. Suppression mechanism of electron emission under fast cluster impact on solids : H. Arai, H. Kudo, S. Tomita, S. Ishii (University of Tsukuba)
45. PIXE analyses of fluid inclusions with a 1-MV tandetron accelerator at University of Tsukuba : M. Kurosawa, K. Sasa, S. Ishii (University of Tsukuba)

Annual meeting of UTTAC users :
Ion-beam based interdisciplinary studies
 15 March, 2010
 Laboratory of Advanced Research B 0110

Oral presentation

1. Application of ion-implantation-induced structural changes to optical devices : M. Fujimaki (National Institute of Advanced Industrial Science and Technology (AIST))
2. Mass measurements of unstable nuclei and quests of uranium nucleosynthesis : A. Ozawa (Graduate School of Pure and Applied Sciences, Univ. of Tsukuba)
3. Long-term denudation of karst landscape: quantification with cosmogenic ³⁶Cl in calcite : Y. Matsushi (MALT, Univ. of Tokyo)
4. Combinatorial PCT measurement of hydrogen storage materials by ion beam : D. Sekiba (UTTAC, Univ. of Tsukuba)
5. The Super Omega muon beamline at J-PARC - High intense new muon source : Y. Ikedo (KEK)

Poster session

1. Cosmogenic ³⁶Cl record in an ice core at the Dome Fuji station, Antarctica : K. Sasa, Y. Matsushi^A, Y. Tosaki^B, T. Takahashi, K. Kurosumi^C, T. Amano^C, J. Kitagawa^C, N. Kinoshita, M. Matsumura, S. Abe, Y. Takaya, K. Sueki^D, Y. Nagashima, K. Bessho^E, H. Matsumura^E, K. Horiuchi^F, H. Matsuzaki^A, H. Motoyama^G (UTTAC, Univ. of Tsukuba, ^AMALT, Univ. of Tokyo, ^BGraduate School of Life and Environmental Sciences, Univ. of Tsukuba, ^CAMS group, Univ. of Tsukuba, ^DRadioisotope center, Univ. of Tsukuba, ^EKEK, FHirosaki Univ., ^GNational institute of polar research)
2. Measurement of ³⁶Cl in soil : Study of extraction methods according to reservoirs : T. Amano, K. Sueki^A, J. Kitagawa, K. Sasa^B, Y. Nagashima^B, T. Takahashi^B, Y. Takaya^B, Y. Matsushi^C, Y. Tosaki^D, N. Kinoshita^B, K. Bessho^E, H. Matsumura^E (AMS Group, University of Tsukuba, ^AUTTAC, University of Tsukuba, ^BRadioisotope center, Univ. of Tsukuba, ^CMALT, Univ. of Tokyo, ^DGraduate School of Life and Environmental Sciences, Univ. of Tsukuba, ^EKEK)
3. Chlorine-36 produced in muon irradiation : N. Kinoshita, K. Sasa, H. Matsumura^A, A. Leveling^B, D. Boehnlein^B (UTTAC, Univ. of Tsukuba, ^AKEK, ^BFermi Lab)

4. Variations of $^{36}\text{Cl}/\text{Cl}$ in precipitation and ^{36}Cl deposition flux : Y. Tosaki, N. Tase, K. Sasa^A, T. Takahashi^A, Y. Nagashima^A (Graduate School of Life and Environmental Sciences, Univ. of Tsukuba, ^AUTTAC, Univ. of Tsukuba)
5. The developments of detectors of the particle identification for the RI beam experiments : T. Moriguchi, A. Ozawa (Graduate School of Pure and Applied Sciences, Univ. of Tsukuba)
6. Measurement of nuclear magnetic moment of unstable nucleus ^{30}P : Y. Abe, A. Ozawa (Graduate School of Pure and Applied Sciences, Univ. of Tsukuba)
7. Measurement of nuclear magnetic moment of unstable nuclei ^{40}Sc : Y. Ishibashi, A. Ozawa (Graduate School of Pure and Applied Sciences, Univ. of Tsukuba)
8. Nucleosynthesis studied by in-beam gamma-ray spectroscopy : T. Komatsubara (UTTAC, Univ. of Tsukuba)
9. Performance Evaluation of CNS Active Targets : S. Ota, T. Hashimoto (Center for Nuclear Study, Univ. of Tokyo)
10. Micro-PIXE analysis of trace elements in single fluid-inclusions using a tandemron accelerator : M. Kurosawa, K. Sasa^A, S. Ishii^A (Graduate School of Life and Environmental Sciences, Univ. of Tsukuba, ^AUTTAC, Univ. of Tsukuba)
11. Fabrication and Mossbauer study of iron nitride nano-particles : M. Minagawa, M. Kishimoto, H. Yanagihara, E. Kita (Graduate School of Pure and Applied Sciences, Univ. of Tsukuba)
12. Nitrogen distribution in ferromagnetic iron-nitride thin films synthesized by an ammonia nitridation method : K. Watanabe, M. Minagawa, D. Sekiba^A, H. Yanagihara, E. Kita (Graduate School of Pure and Applied Sciences, Univ. of Tsukuba, ^AUTTAC, Univ. of Tsukuba)
13. Toward crystalline high-efficiency thin-film solar cells using semiconducting silicide : T. Sue-masu, M. Suzuno, T. Saito, K. Akutsu, H. Kawakami (Graduate School of Pure and Applied Sciences, Univ. of Tsukuba)
14. Anomalous properties of metal nano-clusters interacting with the graphite surface : T. Kondo, J. Oh, D. Hatake, T. Suzuki, Y. Honma, T. Machida, K. Arakawa, D. Sekiba^A, H. Kudo, J. Nakamura (Graduate School of Pure and Applied Sciences, Univ. of Tsukuba, ^AUTTAC, Univ. of Tsukuba)
15. Electric conductivity of hydrogen-doped ITO thin film : D. Sekiba, S. Kohiki^A (UTTAC, Univ. of Tsukuba, ^AKyushu Institute of Technology)
16. Fabrication of all solid state switchable mirror : Y. Shiotani, D. Sekiba (UTTAC, Univ. of Tsukuba)
17. Vicinage effect on energy loss of C_2^+ in thin carbon foil : S. Tamura, K. Kurita, H. Tanikawa, Y. Narita, S. Tomita, S. Ishii^A, K. Sasa^A, H. Kudo (Graduate School of Pure and Applied Sciences, Univ. of Tsukuba, ^AUTTAC, Univ. of Tsukuba)
18. Measurement of resonant coherent excitation with backward electron spectroscopy : Y. Narita, K. Kurita, H. Tanikawa, S. Tamura, S. Tomita, H. Kudo (Graduate School of Pure and Applied Sciences, Univ. of Tsukuba)
19. Nucleation of nano droplets in $\text{N}_2/\text{H}_2\text{O}/\text{SO}_2$ under irradiation of proton beam : H. Tanikawa, M. Matsuoka, K. Kurita, S. Tamura, Y. Narita, Y. Nakai^A, H. Ohara^B, K. Sasa^C, S. Tomita, H. Kudo (Graduate School of Pure and Applied Sciences, Univ. of Tsukuba, ^ARIKEN, ^BNational Institute of Advanced Industrial Science and Technology (AIST), ^CUTTAC, Univ. of Tsukuba)

10. LIST OF PERSONNEL

Tandem Accelerator Complex

H. Kudo	Director, Professor
T. Komatsubara	Assistant Professor
K. Sasa	Assistant Professor
D. Sekiba	Assistant Professor
S. Ishii	Mechanical Engineer
H. Kimura	Computer Engineer
H. Oshima	Electric Engineer
Y. Tajima	Mechanical Engineer
T. Takahashi	Electric Engineer
Y. Yamato	Electric Engineer
N. Kinoshita	Research Fellow
T. Aoki	Research Supporter
K. Iitake	Administrative Staff

Research Members ¹

Inst. of Physics

I. Arai	T. Komatsubara	D. Nagae	A. Ozawa	K. Sasa
H. Suzuki	Y. Takaya			

Inst. of Applied Physics

S. Aoki	K. Akimoto	E. Kita	H. Kudo	T. Suemasu
S. Tomita	A. Uedono	H. Yanagihara		

Inst. of Materials Science

T. Kondo	J. Nakamura
----------	-------------

Inst. of Engineering Mechanics and Systems

K. Matsuuchi

Inst. of Geoscience

M. Kurosawa	N. Tase	Y. Tosaki
-------------	---------	-----------

Inst. of Chemistry

K. Sueki

Staff of Open Advanced Facilities Initiative

M. Matsumura	S. Mihara	H. Muromachi	H. Naramoto	T. Oki
K. Tagishi				

¹The "research members" include the authors and coauthors within 5 years back from this fiscal year, as well as the members of research projects running at UTTAC.

Graduate students

Doctoral Programs of Pure and Applied Science

M. Iijima M. Minagawa T. Moriguchi K. Yamaguchi

Master's Programs of Pure and Applied Science

T. Amano M. Horikoshi T. Ikuyama Y. Ishibashi Y. Ito
T. Kayano M. Matsuoka K. Ogawa H. Ooishi Y. Sakaoka
S. Sato K. Shiba T. Watanabe K. Yokoyama T. Yoshikawa

Undergraduates

Y. Abe T. Ishii N. Kamiguchi S. Kijima J. Kitagawa
Y. Kondo S. Kubota K. Kurita K. Kurosumi S. Mizuno
Y. Narita K. Oda Y. Shiotani Y. Sugiyama H. Tanigawa
S. Tamura Y. Watahiki Y. Watanabe

Scientific Guests and Fellows

K. Awazu	National Institute of Advanced Industrial Science and Technology
M. Fujimaki	National Institute of Advanced Industrial Science and Technology
S.J. Yu	Waseda Univ.
T. Kato	Waseda Univ.
K. Sato	Waseda Univ.
K. Nomura	Waseda Univ.
S. Fujii	Waseda Univ.
A. Yoshida	Waseda Univ.
A. Isaki	Waseda Univ.
Y. Matsushi	Univ. of Tokyo
T. Hayakawa	Japan Atomic Energy Agency
T. Shizuma	Japan Atomic Energy Agency
Y. Ohura	Tokyo Metropolitan Univ.
Y. Hamanaka	Tokyo Metropolitan Univ.
Y. Sasaki	Tokyo Metropolitan Univ.
N. Imamura	Tokyo Metropolitan Univ.
S. Kubono	Center for Nuclear Study, Univ. of Tokyo
H. Yamaguchi	Center for Nuclear Study, Univ. of Tokyo
T. Hashimoto	Center for Nuclear Study, Univ. of Tokyo
S. Hayakawa	Center for Nuclear Study, Univ. of Tokyo
D. Kahl	Center for Nuclear Study, Univ. of Tokyo
D.N. Binh	Center for Nuclear Study, Univ. of Tokyo
H. Hamagaki	Center for Nuclear Study, Univ. of Tokyo
T. Uesaka	Center for Nuclear Study, Univ. of Tokyo
S. Michimasa	Center for Nuclear Study, Univ. of Tokyo
S. Gunji	Center for Nuclear Study, Univ. of Tokyo
S. Ohta	Center for Nuclear Study, Univ. of Tokyo
T. Tokieda	Center for Nuclear Study, Univ. of Tokyo
K. Kawase	Center for Nuclear Study, Univ. of Tokyo
R. Akimoto	Center for Nuclear Study, Univ. of Tokyo
K. Setoodehnia	McMaster Univ.
F. Carpino	McMaster Univ.
K. Fukutani	Univ. of Tokyo
H. Yonemura	Univ. of Tokyo
H. Tsuchida	Kyoto Univ.
K. Nishimura	Kyoto Univ.
R. Murakoshi	Kyoto Univ.
T. Kawahata	Kyoto Univ.